Ocean Engineering 355 (2026) 125065

Contents lists available at ScienceDirect

Ocean Engineering

journal homepage: www.elsevier.com/locate/oceaneng

Research paper

On the singularity and numerical instability of flow fields associated with the nonlinear Schrödinger equation

Marten Hollm *, Robert Seifried

Institute of Mechanics and Ocean Engineering, Hamburg University of Technology, Eissendorfer Strasse 42, Hamburg, 21073, Germany

ARTICLE INFO

Keywords:
Nonlinear Schrödinger equation
Deep-water waves
Flow field
Velocity potential
Singularity
Numerical instability

ABSTRACT

The nonlinear Schrödinger equation (NLS) is a well-known equation in the study of wave motion. In the context of nonlinear water waves, the NLS has been proven to accurately model deep-water waves with a narrow spectral bandwidth and moderate wave steepness. While many studies have focused on reconstructing free surface profiles using the NLS, the associated flow field within the fluid has received less attention. Recently, a paper was published in which the flow field associated with solutions of the NLS was constructed. Here, it has been noted that the associated modeled flow field can contain singularities below the water surface. This work analyzes the occurrence and location of such artificial singularities for different analytical NLS solutions. It is found that the flow field can generally become singular at any depth below the surface and may even appear periodically in water depth. Additionally, it is shown that the numerical computation of the flow field poses considerable challenges due to the instability of numerical schemes. These findings are crucial for the accurate analysis of flow fields corresponding to the NLS.

1. Introduction

For the construction of mechanical structures operating in the ocean, appropriate safety limits have to be determined. Therefore, the magnitude and temporal behavior of the hydrodynamic forces acting on these structures have to be investigated. To model these forces as realistically as possible, the corresponding water waves and fluid behavior have to be modeled accurately.

In general, the behavior of fluids can be described using the Navier-Stokes equations. In theory, this set of equations can handle very complex phenomena with almost no limitations (Lin, 2008). However, solving this set of equations requires significant computational resources, often requiring high-performance computer facilities and well-trained staff (Greaves and Iglesias, 2018). This is particularly problematic for stochastic sea states since, for example, many simulations with long simulation times are required to accurately describe the dynamics of a structure in random waves.

However, for many applications, it is often sufficient to compute the fluid behavior using the potential flow theory (Lin, 2008; Greaves and Iglesias, 2018). Models based on this theory can describe the behavior of homogeneous, incompressible, irrotational, and inviscid fluids, where surface tension effects are neglected. On the other side, since the nonlinear governing equations of potential flow theory involve nonlinear boundary conditions at the unknown free sea surface, solving them requires too much computation time to be heavily applied in the design of offshore structures (Shao et al., 2022). However, Zakharov (1968) has shown that solutions of the nonlinear governing equations of potential flow theory can be reduced to solutions of the nonlinear Schrödinger equation (NLS), which is a partial differential equation for the wave envelope ψ of the water waves. The NLS can be used to accurately model nonlinear deep-water water waves with a narrow spectral bandwidth and moderate wave steepness, see e.g. Dysthe (1979), Osborne (2010), Witt (2019). In addition to water waves, the NLS can be used to describe the propagation of waves in many different physical systems, such as Bose-Einstein condensates (Bludov et al., 2009), fiber optics (Dudley et al., 2014), and plasma waves (El-Tantawy et al., 2022).

Although the NLS is relatively simple, it accounts for both nonlinearity and linear dispersion. Despite its relative simplicity, the NLS describes the nonlinear evolution in time and space of propagating wave packets (Chabchoub, 2013). Furthermore, the NLS captures the Benjamin-Feir instability (Osborne, 2010), which strongly demonstrates the need for nonlinear equations in modeling surface gravity wave propagation.

Compared to the nonlinear governing equation of the potential flow theory, the NLS has several advantages. For example, numerous analytical solutions of the NLS have been presented, see e.g. Peregrine (1983), Osborne (2010), Chabchoub (2013), Slunyaev et al. (2013), Carter et al. (2020) and the references therein. Furthermore, it has been found that

---

* Corresponding author.
E-mail address: marten.hollm@tuhh.de (M. Hollm).

https://doi.org/10.1016/j.oceaneng.2026.125065
Received 19 November 2025; Received in revised form 2 March 2026; Accepted 11 March 2026

the NLS can describe many characteristics of the dynamics of rogue waves, which are found to arise as a result of nonlinear self-focusing phenomena (Onorato et al., 2001). Additionally, it has been conjectured in different studies that specific solutions of the NLS are prototypes of rogue ocean waves, see e.g. Dysthe and Trulsen (1999), Shrira and Geogjaev (2010), Dostal et al. (2020). Moreover, numerical solutions of the NLS can be computed much more efficiently than solutions of the nonlinear governing equation of the potential flow theory. Finally, irregular sea states can be efficiently generated using the NLS by employing the approach presented in Hollm et al. (2021, 2022).

Although many studies have investigated the reconstruction of the free surface profile and the accuracy of such profiles predicted by the NLS for ocean waves, comparatively few works have focused on the associated flow field inside the fluid. In this way, Carter et al. (2020) have derived a general representation for the corresponding velocity potential ϕ. Based on ϕ, they have investigated the trajectories of water particles inside the fluid using the NLS. However, without much comment, Carter et al. (2020) have noticed that the velocity potential ϕ corresponding to solutions ψ of the NLS can have singularities at $z = \mathcal{O}\left(\varepsilon^{-1}\right)$, whereby z denotes the vertical space-coordinate and ε is the wave steepness of the corresponding waves. This is surprising, as even experiments have shown that the NLS can be used to model specific kinds of water waves, see e.g. Chabchoub (2013), Slunyaev et al. (2013), Chabchoub et al. (2012).

Although Carter et al. (2020) have observed the occurrence of singularities in ϕ, the origin and the exact location of these singularities are still unknown. Consequently, Carter et al. (2020) have considered only the trajectories of water particles sufficiently close to the fluid surface and far away from the singularities. However, for many applications, it is necessary to compute the flow field of the water waves in greater water depths. For example, a new computational method has been presented and analyzed in Hollm and Seifried (2026) that uses the NLS to calculate the fluid-structure interaction between mechanical structures and nonlinear ocean waves. Especially when considering mechanical structures that extend deep into the ocean, it is important to know whether, and where, the velocity potential ϕ corresponding to solutions ψ of the NLS becomes singular below the sea surface, as these singularities can affect the results of the fluid-structure interaction.

A second problem occurs in the numerical computation of the velocity potential ϕ. The formula of Carter et al. (2020) for ϕ shows that a complex transport equation has to be solved to compute ϕ numerically, if no analytical solution ψ of the NLS is available. However, the numerical stability of the corresponding solution schemes poses a significant challenge when numerically solving this equation.

Therefore, two big issues arise when computing the velocity potential ϕ corresponding to solutions ψ of the NLS: the occurrence of singularities of the velocity potential ϕ below the sea surface, and stability issues in the numerical computation of ϕ. These challenges have important practical consequences for marine engineering applications. Specifically, they may lead to inaccurate or biased predictions of hydrodynamic loads and fluid motion characteristics, which are critical parameters for the design and safety assessment of offshore structures. As the two aforementioned issues become more relevant at greater depths below the water surface, such inaccuracies are particularly consequential for deep-drafted offshore structures. Hence, addressing these mathematical and numerical issues in the computation of the velocity potential ϕ is essential to ensure reliable simulations and robust engineering decisions in offshore design processes.

In this work, the two aforementioned big issues in the computation of the velocity potential ϕ corresponding to solutions ψ of the NLS are analyzed. By examining several exemplary analytical solutions ψ of the NLS, the occurrence and location of singularities in the corresponding velocity potentials ϕ are investigated. Specifically, the following questions are addressed: Can the velocity potential ϕ become singular at some water depth for every solution ψ of the NLS? For different analytical solutions ψ of the NLS, where does the corresponding velocity potential ϕ become singular? Does a water depth $\bar{z} < 0$ exist such that the velocity potential ϕ can be computed without any singularities for $z \in (\bar{z}, 0]$ for all solutions ψ of the NLS? Furthermore, different numerical schemes are analyzed with respect to their stability when applied to the complex transport equation. In this way, attention shall be drawn to problems that need to be taken into account in the calculation of the flow field associated with solutions ψ of the NLS.

The work is organized as follows: First, the derivation of the NLS is briefly reviewed in Section 2. Based on the solution ψ of the NLS, it is also presented how the corresponding sea surface displacement η and velocity potential ϕ can be computed. Afterward, the behavior of the velocity potential ϕ below the sea surface is investigated in Section 3. Here, different analytical solutions ψ of the NLS are presented and analyzed with regard to singularities in the corresponding velocity potential ϕ. In Section 4, different numerical schemes are presented to compute ϕ in the absence of any analytical solution ψ of the NLS. Here, the numerical stability of the different schemes is investigated. Finally, this work ends with a conclusion in Section 5.

2. Modeling of water waves using the NLS

In this section, the derivation of the NLS is sketched, and the construction of the corresponding velocity potential ϕ is briefly outlined. For details, it is refereed to Carter et al. (2020), Hollm (2025). In this work, the behavior of homogeneous, incompressible, inviscid, and irrotational fluids is considered, whereby surface tension is neglected. Let x and z denote the respective horizontal and vertical spatial variables, and t the time variable. The plane of the undisturbed free sea surface is located at $z = 0$, and the z-axis is positive upwards. Only long-crested waves are considered propagating in x-direction. The vertical displacement of any point on the free sea surface at time t and space x is given by $z = \eta = \eta(x, t)$. Here, it is assumed that the water waves are not breaking such that the value of $\eta(x, t)$ is uniquely defined everywhere.

Using the assumptions mentioned above, the fluid motion can be described by the velocity potential $\phi = \phi(x, z, t)$. The governing equations of fluid motion of potential flow theory are given by

$$\nabla^2 \phi = \phi_{xx} + \phi_{zz} = 0, \qquad \text{for} \quad \infty < z < \eta(x, t), \tag{1a}$$

$$\eta_t + \phi_x \eta_x = \phi_z, \qquad \text{at} \quad z = \eta(x, t), \tag{1b}$$

$$\phi_t + \frac{1}{2} \nabla\phi \cdot \nabla\phi + g\eta = 0, \qquad \text{at} \quad z = \eta(x, t), \tag{1c}$$

$$\phi_z \to 0, \qquad \text{as} \quad z \to -\infty, \tag{1d}$$

see e.g. Carter et al. (2020), Newman (2018). Here, ∇ denotes the nabla operator in space, and g is the gravitational constant. It has to be noted that the external pressure exerted on the sea surface η is assumed to be zero.

After calculating the velocity potential ϕ and the sea surface displacement η by solving Eq. (1), the dynamics of water waves on the open sea can be calculated. However, solving Eq. (1) requires significant computational effort due to the two nonlinear boundary conditions (BCs) at the unknown position of the free sea surface $z = \eta$. In order to reduce this effort, η and ϕ can be computed using the NLS. In the following, the derivation of the NLS is shortly outlined, and the resulting formulas for η and ϕ corresponding to solutions of the NLS are presented. More details about the derivation of the NLS can be found, for example, in Dysthe (1979), Carter et al. (2020), Hollm (2025), Mei (1983).

2.1. Derivation of the NLS

In the derivation of the NLS, it is first used that the two BCs (1b) and (1c) at the free sea surface $z = \eta$ can be replaced by one single BC at $z = \eta$. To this end, the substantial derivative of Eq. (1c) is considered (Newman, 2018), i. e.

$$\left(\frac{\partial}{\partial t} + \nabla\phi \cdot \nabla\right)\left[\phi_t + \frac{1}{2}\nabla\phi \cdot \nabla\phi + g\eta\right] = 0, \quad \text{for} \quad z = \eta(x, y, t). \tag{2}$$

Here, the substantial derivative expresses the time rate-of-change in a coordinate system moving with the fluid. Using Eq. (1b), Eq. (2) can be rewritten to, see e.g. Mei (1983), Newman (2018),

$$\phi_{tt} + g\phi_z + 2\nabla\phi\cdot\nabla\phi_t + \frac{1}{2}\nabla\phi\cdot\nabla(\nabla\phi\cdot\nabla\phi) = 0, \quad \text{for} \quad z = \eta(x,y,t). \tag{3}$$

This BC is exact and only depends on ϕ, except that it has to be applied at the unknown sea surface position $z = \eta$.

Next, Taylor series expansions are employed to expand Eq. (3) and Eq. (1c) from $z = \eta$ to $z = 0$. Considering only the terms up to third order in the product of ϕ, η, and their derivatives, the expanded equations evaluated at $z = 0$ become

$$\begin{aligned}\phi_{tt} + g\phi_z + \eta\frac{\partial}{\partial z}\left[\phi_{tt} + g\phi_z\right] + 2\nabla\phi\cdot\nabla\phi_t + \frac{1}{2}\eta^2\frac{\partial^2}{\partial z^2}\left[\phi_{tt} + g\phi_z\right]\\ +\eta\frac{\partial}{\partial z}\left[2\nabla\phi\cdot\nabla\phi_t\right] + \frac{1}{2}\nabla\phi\cdot\nabla(\nabla\phi\cdot\nabla\phi) = 0,\end{aligned} \tag{4a}$$

$$-g\eta = \phi_t + \eta\phi_{tz} + \frac{1}{2}\nabla\phi\cdot\nabla\phi + \frac{1}{2}\eta^2\phi_{tzz} + \eta\frac{\partial}{\partial z}\left[\frac{1}{2}\nabla\phi\cdot\nabla\phi\right]. \tag{4b}$$

These equations have also been presented, for example, in Mei (1983).

Afterward, the velocity potential ϕ and sea surface displacement η are described using the modulated wave train ansatz, see Carter et al. (2020),

$$\phi(x,z,t) = \bar{\phi} + \varepsilon A_1 e^{k_0 z + i(k_0 x - \omega_0 t)} + \varepsilon^2 A_2 e^{2\left(k_0 z + i(k_0 x - \omega_0 t)\right)} + \dots + \text{c.c.}, \tag{5a}$$

$$\eta(x,t) = \bar{\eta} + \varepsilon B e^{i(k_0 x - \omega_0 t)} + \varepsilon^2 B_2 e^{2i(k_0 x - \omega_0 t)} + \varepsilon^3 B_3 e^{3i(k_0 x - \omega_0 t)} + \dots + \text{c.c.} \tag{5b}$$

Here, the perturbation parameter ε represents the wave steepness $k_0 A_0$ of the carrier wave with wave number k_0 and a typical wave amplitude A_0. Moreover, ω_0 represents the corresponding wave frequency of the carrier wave, and c.c. represents the complex conjugate. Furthermore, as described in Carter et al. (2020), it is assumed

$$\bar{\phi} = \bar{\phi}(X,Z,T) = \varepsilon^2\bar{\phi}_0(X,Z,T) + \varepsilon^3\bar{\phi}_1(X,Z,T) + \varepsilon^4\bar{\phi}_2(X,Z,T) + \dots, \tag{6a}$$

$$\begin{aligned}A_j = A_j(X,Z,T) &= A_{j0}(X,Z,T) + \varepsilon A_{j1}(X,Z,T)\\ &+ \varepsilon^2 A_{j2}(X,Z,T) + \dots, \quad \text{for } j = 1,2,3,\dots,\end{aligned} \tag{6b}$$

$$\bar{\eta} = \bar{\eta}(X,T) = \varepsilon^3\bar{\eta}_0(X,T) + \varepsilon^4\bar{\eta}_1(X,T) + \varepsilon^5\bar{\eta}_2(X,T) + \dots, \tag{6c}$$

$$B = B(X,T), \tag{6d}$$

$$\begin{aligned}B_j = B_j(X,Z,T) &= B_{j0}(X,Z,T) + \varepsilon B_{j1}(X,Z,T)\\ &+ \varepsilon^2 B_{j2}(X,Z,T) + \dots, \quad \text{for } j = 2,3,4,\dots\end{aligned} \tag{6e}$$

Here, X, Z, and T are the slow variables defined by

$$X := \varepsilon x, \quad Z := \varepsilon z, \quad \text{and} \quad T := \varepsilon t. \tag{7}$$

The expressions from Eqs. (5) and (6) are substituted into the Laplace Eq. (1a) and the BCs (4a) and (4b) at $z = 0$. This yields terms of various orders in ε and $e^{k_0 z \pm i(k_0 x - \omega_0 t)}$, which are analyzed separately. The resulting PDEs and BCs at $Z = 0$ for the unknowns A_{ij}, which appear in Eq. (5) up to the order $O(\varepsilon^3)$, and $\bar{\phi}_0$ are given by

$$\begin{cases} A_{10,Z} + iA_{10,X} = 0, \quad \text{for } Z < 0,\\ A_{10} = -\frac{i\omega_0}{k_0}B, \quad \text{for } Z = 0,\end{cases} \tag{8a}$$

$$\begin{cases} A_{20,Z} + iA_{20,X} = 0, \quad \text{for } Z < 0,\\ A_{20} = 0, \quad \text{for } Z = 0,\end{cases} \tag{8b}$$

$$\begin{cases} A_{11,Z} + iA_{11,X} = -\frac{1}{2k_0}\left(A_{10,XX} + A_{10,ZZ}\right), \quad \text{for } Z < 0,\\ A_{11} = \frac{\omega_0}{2k_0^2}B_X, \quad \text{for } Z = 0,\end{cases} \tag{8c}$$

$$\begin{cases} A_{30,Z} + iA_{30,X} = 0, \quad \text{for } Z < 0,\\ A_{30} = 0, \quad \text{for } Z = 0,\end{cases} \tag{8d}$$

$$\begin{cases} A_{21,Z} + iA_{21,X} = -\frac{1}{4k_0}\left(A_{20,XX} + A_{20,ZZ}\right), \quad \text{for } Z < 0,\\ A_{21} = 0, \quad \text{for } Z = 0,\end{cases} \tag{8e}$$

$$\begin{cases} A_{12,Z} + iA_{12,X} = -\frac{1}{2k_0}\left(A_{11,XX} + A_{11,ZZ}\right), \quad \text{for } Z < 0,\\ A_{12} = \frac{1}{2}ik_0\omega_0|B|^2B + \frac{3i\omega_0}{8k_0^3}B_{XX}, \quad \text{for } Z = 0,\end{cases} \tag{8f}$$

$$\begin{cases} \bar{\phi}_{0,XX} + \bar{\phi}_{0,ZZ} + \bar{\phi}^*_{0,XX} + \bar{\phi}^*_{0,ZZ} = 0, \quad \text{for } Z < 0,\\ \bar{\phi}_{0,Z} + \bar{\phi}^*_{0,Z} = 2\omega_0\left(|B|^2\right)_X, \quad \text{for } Z = 0.\end{cases} \tag{8g}$$

Here, $\bar{\phi}_0^*$ denotes the complex conjugate of $\bar{\phi}_0$. The corresponding solutions of Eq. (8) are given in terms of B by

$$\begin{aligned}&A_{10} = -\frac{i\omega_0}{k_0}\widetilde{B}, \quad A_{11} = \frac{\omega_0}{2k_0}\widetilde{B}_X, \quad A_{12} = \frac{1}{16}ik_0\omega_0\widetilde{D} + \frac{3i\omega_0}{8k_0^3}\widetilde{B}_{XX},\\ &A_{20} = 0, \quad A_{21} = 0, \quad A_{30} = 0, \quad \bar{\phi}_0(X,Z,T) + \bar{\phi}_0^*(X,Z,T)\\ &= \mathcal{F}^{-1}\left(2i\omega_0\,\mathrm{sgn}(k)\mathcal{F}\left(|B|^2\right)e^{|k|Z}\right)\end{aligned} \tag{9}$$

with $\widetilde{B}(X,Z,T) = B(X - iZ,T)$, $D(X,T) = 8|B(X,T)|^2B(X,T)$, $\widetilde{D}(X,Z,T) = D(X - iZ,T)$. Furthermore, $\mathcal{F}$ denotes the Fourier transform with respect to the coordinate X and $\mathcal{F}^{-1}$ its inverse, which are given by

$$\begin{aligned}\hat{f}(k) = \mathcal{F}(f(X)) &:= \int_{\mathbb{R}} f(X)e^{-ikX}\,dX,\\ f(X) = \mathcal{F}^{-1}\left(\hat{f}(k)\right) &:= \frac{1}{2\pi}\int_{\mathbb{R}} \hat{f}(k)e^{ikX}\,dk.\end{aligned} \tag{10}$$

In addition, the functions B_{ij} and $\bar{\eta}_0 + \bar{\eta}_0^*$, which appear in Eq. (5b) up to the order $\mathcal{O}(\varepsilon^3)$, are given in terms of B by

$$\begin{aligned}&B_{20} = k_0B^2, \quad B_{30} = \frac{3}{2}k_0^2B^3, \quad B_{21} = -ik_0BB_X,\\ &\bar{\eta}_0 + \bar{\eta}_0^* = -\frac{1}{g}\left[\left(\bar{\phi}_0 + \bar{\phi}_0^*\right)_T\right]_{Z=0} = \frac{2\omega_0}{g}\frac{\partial}{\partial T}\left(\mathcal{H}\left(|B|^2\right)\right).\end{aligned} \tag{11}$$

Here, $\mathcal{H}$ denotes the Hilbert transform, which can be computed by $\mathcal{H}(f(X)) = \mathcal{F}^{-1}(-i\,\mathrm{sgn}(k)\mathcal{F}(f))$.

It remains to calculate the function B. For this purpose, the two BCs (4a) and (4b) are combined into a single BC at $Z = 0$ in terms of ϕ by substituting the expression for η from Eq. (4b) into Eq. (4a). In the resulting equation, only the terms up to third order in the products of ϕ and its derivatives are considered. Next, ϕ is replaced by the expression from Eq. (5a), whereby A_{ij} and $\bar{\phi}_0$ are substituted by the expressions given by Eq. (9). Considering only the terms up to order $O(\varepsilon^3)$, it is found that B has to satisfy

$$i\varepsilon^2\left(B_T + \frac{\omega_0}{2k_0}B_X\right) = \varepsilon^3\left(\frac{\omega_0}{8k_0^2}B_{XX} + 2\omega_0k_0^2B|B|^2\right). \tag{12}$$

2.2. *General overview of the resulting NLS equations*

After solving Eq. (12), the corresponding velocity potential ϕ and sea surface displacement η can be calculated by substituting the Eqs. (9) and (11) into Eq. (5). The resulting expressions for η and ϕ can slightly be simplified by substituting $\psi(X,T) = 2B(X,T)$. In this way, it results the NLS

$$i(\psi_T + c_{gr}\psi_X) = \nu\psi_{XX} + \delta|\psi|^2\psi. \tag{13}$$

Here, the constants ν, δ, and the group velocity c_{gr} are defined as

$$\nu := \varepsilon\frac{\omega_0}{8k_0^2}, \quad \delta := \varepsilon\frac{1}{2}\omega_0k_0^2, \quad c_{gr} := \frac{\omega_0}{2k_0}. \tag{14}$$

Furthermore, the wave frequency ω_0 and wave number k_0 of the carrier wave are linked by the linear dispersion relation in deep water, i. e. $\omega_0^2 = gk_0$.

After solving the NLS (13) to compute the wave envelope ψ, the sea surface displacement $\eta(x,t)$ and velocity potential $\phi(x,z,t)$ of the corresponding water waves are given by

$$\eta(x,t) = \mathrm{Re}\left\{ \varepsilon\psi E + \frac{1}{2}\varepsilon^2 k_0 \psi^2 E^2 + \varepsilon^3 \left[\frac{3}{8} k_0^2 \psi^3 E^3 - \frac{1}{2}\mathrm{i}\psi\psi_X E^2 + \frac{\omega_0}{2g}\frac{\partial}{\partial T}\left(\mathcal{H}\left(|\psi|^2\right)\right)\right]\right\} + O(\varepsilon^4), \tag{15}$$

$$\phi(x,z,t) = \mathrm{Re}\left\{ \left[-\frac{\mathrm{i}\varepsilon\omega_0}{k_0}\widetilde{\psi} + \frac{\varepsilon^2\omega_0}{2k_0^2}\widetilde{\psi}_X + \varepsilon^3\left(\frac{\mathrm{i}k_0\omega_0}{8}\widetilde{C} + \frac{3\mathrm{i}\omega_0}{8k_0^3}\widetilde{\psi}_{XX}\right)\right] E\mathrm{e}^{k_0 z} + 2\varepsilon^2\bar{\phi}_0 + 2\varepsilon^3\bar{\phi}_1 \right\} + O(\varepsilon^4). \tag{16}$$

Here, it is $E = \mathrm{e}^{\mathrm{i}(k_0 x - \omega_0 t)}$, $\widetilde{\psi}(X,Z,T) := \psi(X - \mathrm{i}Z, T)$, $C := |\psi|^2\psi$ and $\widetilde{C}(X,Z,T) := C(X - \mathrm{i}Z, T)$. As presented in Hollm and Seifried (2026), Hollm (2025), Hollm et al. (2024), Eq. (16) is the corrected version of the formula by Carter et al. (2020), who did not consider the mean flow velocity potentials $\bar{\phi}_0$ and $\bar{\phi}_1$ in Eq. (16). The velocity potential $\bar{\phi}_0$ is given by

$$\mathrm{Re}\left\{ 2\bar{\phi}_0 \right\} = \bar{\phi}_0 + \bar{\phi}_0^* = \mathcal{F}^{-1}\left(\frac{1}{2}\mathrm{i}\omega_0\,\mathrm{sgn}(k)\mathcal{F}\left(|\psi|^2\right)\mathrm{e}^{|k|Z}\right). \tag{17}$$

It has to be noted that the velocity potential $\bar{\phi}_1$ appearing in Eqs. (6a) and (16) will not further be specified in this work as it has only a small effect on the wave dynamics. As $\bar{\phi}_1$ depends only on $T = \varepsilon t$, $X = \varepsilon x$, and $Z = \varepsilon z$, it holds

$$\bar{\phi}_{1,t} = \varepsilon\bar{\phi}_{1,T}, \quad \bar{\phi}_{1,x} = \varepsilon\bar{\phi}_{1,X}, \quad \bar{\phi}_{1,z} = \varepsilon\bar{\phi}_{1,Z}. \tag{18}$$

Recall that the gradient of the velocity potential ϕ, $\nabla\phi$, computes the velocity of the water at any point in the water domain. Since $\bar{\phi}_1$ is of order $O(\varepsilon^3)$, the derivatives $\bar{\phi}_{1,t}$, $\bar{\phi}_{1,x}$, and $\bar{\phi}_{1,z}$ are of order $O(\varepsilon^4)$. Therefore, considering $\bar{\phi}_1$ only affects the wave dynamics of order $O(\varepsilon^4)$. On the other side, the NLS is derived considering all terms in Eqs. (5) and (6) up to order $O(\varepsilon^3)$. For this reason, the NLS is accurate to the third order in the wave steepness ε. As $\bar{\phi}_1$ only affects the wave dynamics of order $O(\varepsilon^4)$, $\bar{\phi}_1$ is not specified here and will not be considered in the further course of this work.

In summary, after solving the NLS for the wave envelope ψ, the sea surface displacement η and velocity potential ϕ can be computed using Eqs. (15) and (16), respectively. Fig. 1 shows two examples of the wave envelope ψ and the associated sea surface displacement η, whereby only the leading order term in ε is used to calculate η. Here, the wave envelope ψ is used to describe regular and non-regular water waves, see Figs. 1a-1b.

Given the sea surface displacement η and velocity potential ϕ, the dynamics of the water waves and the fluid can be calculated. This allows, for example, the computation and analysis of the water pressure, the trajectories of water particles, and the fluid-structure interaction between ocean waves and mechanical structures in a post-processing step. The entire procedure for using the NLS in fluid dynamics applications is depicted in Fig. 2. As the velocity potential ϕ from Eq. (16) plays an important role here, its behavior below the sea surface is analyzed in the following.

3. Singularities of flow fields associated with analytical solutions of the NLS

Given the solution ψ of the NLS (13), the corresponding velocity potential ϕ can be computed using Eq. (16). Here, it can be seen that the z-dependency of ϕ is strongly related to the behavior of the auxiliary variables $\widetilde{\psi}(X,Z,T)$ and $\widetilde{C}(X,Z,T)$ in water depth $Z = \varepsilon z$. However, by observing the behavior of $\widetilde{\psi}$ and $\widetilde{C}$ with respect to Z, it can be found that $\widetilde{\psi}$ and $\widetilde{C}$ can contain singularities for large values of Z. Therefore, also the velocity potential ϕ from Eq. (16) can contain singularities in the depth Z. Depending on the behavior of $\widetilde{\psi}$ and $\widetilde{C}$ with respect to Z, it also follows that the condition $\phi_z \to 0$ for $z \to -\infty$ from Eq. (1d) might not be fulfilled by the velocity potential ϕ from Eq. (16).

It is important to note that the aforementioned singularities do not result from any physical blowup. Instead, they are mathematical artifacts arising from the reconstruction of the velocity potential ϕ corresponding to solutions of the NLS. Specifically, the reconstruction of ϕ relies on the analytic continuation of the wave envelope ψ and auxiliary variable C from the real spatial coordinate X into the complex plane $X - iZ$. Thus, the functions $\widetilde{\psi}$ and $\widetilde{C}$ are the analytic continuations of the functions ψ and C into the complex plane. Such analytic continuations are valid only up to a certain depth, referred to as the radius of analyticity. Beyond this depth, the reconstruction of the velocity potential ϕ breaks down and singularities appear. Therefore, these singularities do not represent a physical divergence of the underlying inviscid potential flow, but indicate the limited domain of validity of the analytic continuations.

In this section, the behavior of the singularities of $\widetilde{\psi}$ and $\widetilde{C}$ with respect to Z is investigated. This investigation extends the study presented in Carter et al. (2020). For different analytical solutions of the NLS (13), it is studied whether $\widetilde{\psi}$ and $\widetilde{C}$ contain singularities in Z, and if so, where they are located. For this purpose, several analytical solutions of the NLS (13) are presented and their singularities are investigated in Sections 3.1-3.9. In order to simplify the investigation, only the singularities appearing in $\widetilde{\psi}$ are considered here. The corresponding locations of the singularities of $\widetilde{C}$ are discussed in Section 3.10. This section ends with a summary of all results in Section 3.11.

In order to simplify the notation in the following, the normalized dimensionless coordinates

$$r = \psi_0 b(X - c_{\mathrm{gr}}T), \quad s = \psi_0 b Z, \text{ and } \tau = \delta\psi_0^2 T \tag{19}$$

are introduced. Here, r denotes the normalized horizontal coordinate, s the normalized vertical coordinate (depth), and τ the normalized time. In Eq. (19), the constant b is given by

$$b = \sqrt{\frac{\delta}{2\nu}}. \tag{20}$$

3.1. Plane-wave solution

The plane-wave solution of the NLS has an amplitude that is constant in time and space, and is given by

$$\psi(X,T) = \psi_0 \mathrm{e}^{\mathrm{i}k_{\mathrm{pw}}X - \mathrm{i}\left(k_{\mathrm{pw}}c_{\mathrm{gr}} - \nu k_{\mathrm{pw}}^2 + \delta\psi_0^2\right)T}, \tag{21}$$

see e.g. Carter et al. (2020). Here, $\psi_0 \in \mathbb{R}$ is the amplitude of the solution and $k_{\mathrm{pw}} \in \mathbb{R}$ is an arbitrary constant.

The auxiliary variable $\widetilde{\psi}$ corresponding to the plane-wave solution of the NLS is then given by

$$\widetilde{\psi}(X,Z,T) = \psi(X - \mathrm{i}Z, T) = \psi(X,T)\mathrm{e}^{k_{\mathrm{pw}}Z}. \tag{22}$$

Since $Z < 0$, it can be observed that $\widetilde{\psi}$ decays exponentially for an increasing water depth. Consequently, $\widetilde{\psi}$ shows no singularities under water. The same holds for the variable $\widetilde{C}$, which is given by $\widetilde{C}(X,Z,T) = \psi_0^2\widetilde{\psi}(X,Z,T)$. Therefore, the corresponding velocity potential $\phi(x,z,t)$ can be computed for each depth $z < 0$. As will be seen in the further course of this section, the plane wave solution is the only one of the solutions presented here where the corresponding velocity potential ϕ has no singularities in water depth.

3.2. Soliton solution

One important solution of the NLS (13) is an isolated and stationary sech-shape nonlinear wave group on zero background. This solution of the NLS is known as the soliton solution and is given by

$$\psi(X,T) = \psi_0 \mathrm{sech}\left(\psi_0 b\left(X - c_{\mathrm{gr}}T\right)\right)\mathrm{e}^{-\frac{1}{2}\mathrm{i}\delta\psi_0^2 T}, \tag{23}$$

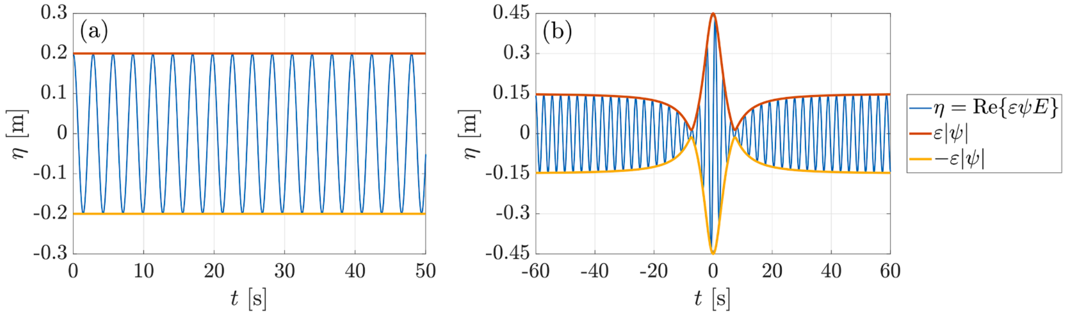

Fig. 1. Relationship between the wave envelope ψ and sea surface displacement η shown for two different solutions of the NLS. Here, (a) regular and (b) non-regular water waves are described using the NLS.

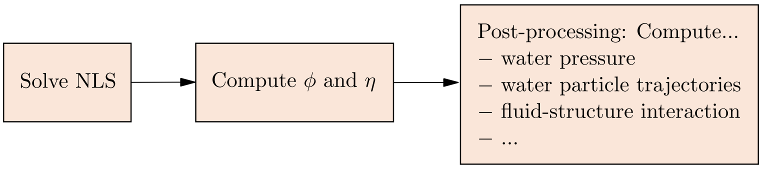

Fig. 2. Flowchart of the use of the NLS in fluid dynamics applications.

see e.g. Slunyaev et al. (2013). Here, $\psi_0 \in \mathbb{R}$ denotes the amplitude of the solution and b is given by Eq. (20). Fig. 3a shows the amplitude of the soliton solution for $k_0 = 0.5\,\mathrm{m}^{-1}$, $\psi_0 = 1\,\mathrm{m}$, and $\varepsilon = 0.1$ with respect to the moving coordinate $\xi = X - c_{\mathrm{gr}}T$. It can be seen that the solution represents a wave packet on an otherwise calm sea surface. The shape of the envelope of the wave packet remains unchanged in propagation.

Considering the dimensionless coordinates r, s, and τ from Eq. (24), the corresponding auxiliary variable $\widetilde{\psi}$ is given by

$$\widetilde{\psi}(X, Z, T) = \psi_0 \operatorname{sech}(r - \mathrm{i}s)\mathrm{e}^{-\frac{1}{2}\mathrm{i}\tau}. \tag{24}$$

In order to investigate whether $\widetilde{\psi}$ contains any singularity, it has to be noted that the relation

$$\operatorname{sech}(r - \mathrm{i}s) = \frac{1}{\cosh(r - \mathrm{i}s)} = \frac{1}{\cosh(r)\cos(s) - \mathrm{i}\sinh(r)\sin(s)} \tag{25}$$

holds. This term gets singular for

$$r = 0 \quad \text{and } s = \frac{\pi}{2}(2n+1), n \in \mathbb{Z}. \tag{26}$$

Therefore, it is observed that $\widetilde{\psi}$ contains poles periodically in s and Z, respectively. From this, it also follows that the condition $\phi_z \to 0$ for $z \to -\infty$ from Eq. (1d) is not fulfilled by the velocity potential ϕ corresponding to the soliton solution of the NLS.

The (ξ, T)-location of the singularity of the soliton solution is highlighted in red in Fig. 3a. For a given time $T \in \mathbb{R}$, it can be seen that the poles are located below the position where the wave envelope ψ of the soliton solution has its maximal amplitude in space. To visualize the behavior of $\widetilde{\psi}$ below the still water surface, Fig. 3b shows the amplitude of $\widetilde{\psi}$ at $r = \xi = 0$ over the normalized coordinate s. The s-coordinates of the poles from Eq. (26) can directly be recognized in Fig. 3b.

Regarding the velocity potential ϕ corresponding to the NLS (13), it can be concluded that, starting from the mean sea level at $z = 0$, the velocity potential ϕ can only be computed below the still water surface down to the depth of the first pole. For $n = -1$ and substituting b, v and δ from Eqs. (20) and (14) into Eq (26) and by transforming the coordinate s back to Z using Eq. (19), it is found that the velocity potential $\phi(x, z, t)$ corresponding to the soliton solution of the NLS (13) can be computed without any singularity only for depths

$$z = \frac{Z}{\varepsilon} > z_{\mathrm{Sol}} := -\frac{\pi}{2\varepsilon b\psi_0} = -\frac{\pi}{2\sqrt{2}\varepsilon\psi_0 k_0^2}. \tag{27}$$

This has to be taken into account when working with the flow field of water waves corresponding to the soliton solution of the NLS.

3.3. *Cnoidal-wave solution*

The cnoidal-wave solution of the NLS (13) is given by

$$\psi(X, T) = \psi_0 \operatorname{cn}\left(\frac{\psi_0}{\kappa} b\left(X - c_{\mathrm{gr}}T\right), \kappa\right)\mathrm{e}^{-\frac{1}{2}\mathrm{i}\delta\psi_0^2\frac{2\kappa^2-1}{\kappa^2}T}, \tag{28}$$

see e.g. Carter et al. (2020). Here, ψ_0 denotes the amplitude of the wave, $\kappa \in (0, 1]$ is a real-valued parameters and b is given by Eq. (20). Furthermore, $\operatorname{cn}(\cdot, \kappa)$ is the Jacobi-elliptic function with elliptic modulus κ. Fig. 4a shows the amplitude of the cnoidal-wave solution for $k_0 = 0.5\,\mathrm{m}^{-1}$, $\psi_0 = 1\,\mathrm{m}$, $\varepsilon = 0.1$, and $\kappa = 0.8$ with respect to the moving coordinate $\xi = X - c_{\mathrm{gr}}T$. It can be seen that the cnoidal-wave solution represents a wave, where the shape of the envelope remains unchanged in propagation direction.

Note that for $\kappa = 1$, it holds $\operatorname{cn}(\cdot, 1) = \operatorname{sech}(\cdot)$ and the cnoidal-wave solution from Eq. (28) becomes the soliton solution from Eq. (23). Therefore, the cnoidal-wave solution from Eq. (28) can be seen as a generalization of the soliton solution from Eq. (23).

In terms of the dimensionless coordinates r, s and τ, the corresponding auxiliary variable $\widetilde{\psi}$ is given by

$$\widetilde{\psi}(X, Z, T) = \psi_0 \operatorname{cn}\left(\frac{r - \mathrm{i}s}{\kappa}, \kappa\right)\mathrm{e}^{-\frac{1}{2}\mathrm{i}\frac{2\kappa^2-1}{\kappa^2}\tau}. \tag{29}$$

In order to investigate whether $\widetilde{\psi}$ contains any singularity, it has to be noted that the Jacobi-elliptic function $\operatorname{cn}(\zeta, \kappa)$ has the poles $\zeta = 2mK(\kappa) + (2n+1)\mathrm{i}K'(\kappa) \in \mathbb{C}$. Here, $m, n \in \mathbb{Z}$, K is the complete elliptic integral of first kind defined by

$$K(\kappa) = \int_0^{\pi/2} \frac{1}{\sqrt{1 - \kappa^2 \sin(\varphi)}}\mathrm{d}\varphi, \tag{30}$$

and $K'(\kappa) = K(\kappa')$ with the complementary parameter $\kappa' = \sqrt{1 - \kappa^2}$. Applied on Eq. (29), it results that $\widetilde{\psi}$ has poles for

$$r = 2m\kappa K(\kappa) \quad \text{and} \quad s = -(2n+1)\kappa K'(\kappa), \quad m, n \in \mathbb{Z}. \tag{31}$$

It can be seen that $\widetilde{\psi}$ contains poles periodically in r and s. In r-direction, $\widetilde{\psi}$ contains poles at the locations where the wave envelope ψ has its maximum. This is also shown in Fig. 4a, where the (ξ, T)-location of the poles is highlighted in red.

In s-direction, the locations of the poles of $\widetilde{\psi}$ depend on κ. This is also presented in Figs. 4b-4c. Here, the amplitude of $\widetilde{\psi}$ is shown against s for $k_0 = 0.5\,\mathrm{m}^{-1}$, $\psi_0 = 1\,\mathrm{m}$, $\varepsilon = 0.1$, and two different values of κ, namely $\kappa = 0.2$ and $\kappa = 0.8$, at $r = 0$. The s-coordinates of the first three poles,

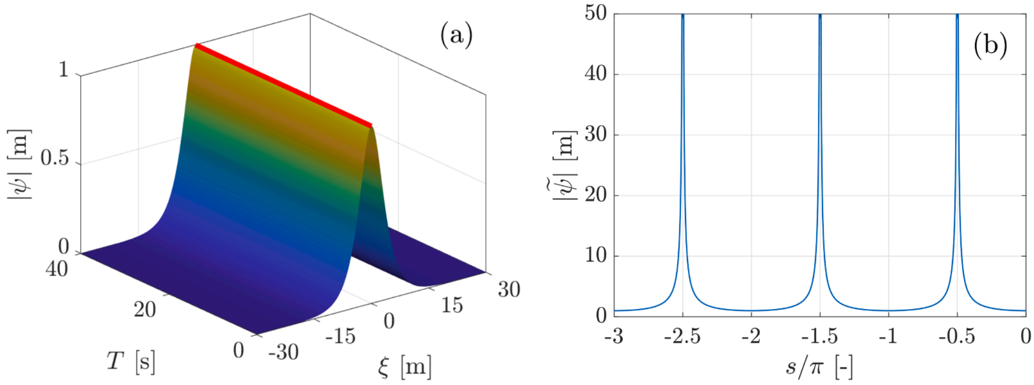

Fig. 3. (a): Amplitude of wave envelope ψ of the soliton solution including the (ξ, T)-location of the singularity (red). (b): Amplitude of the corresponding auxiliary variable $\widetilde{\psi}$ at $r = \xi = 0$ over the normalized depth coordinate s.

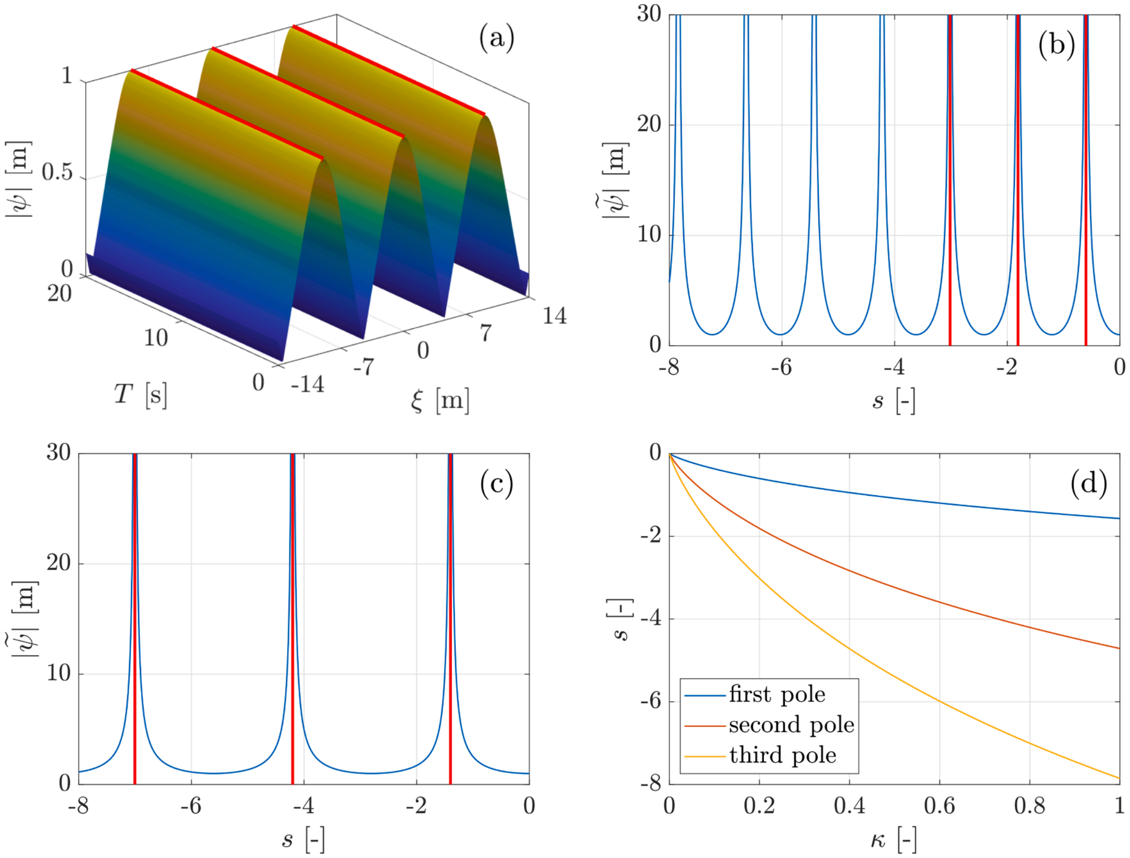

Fig. 4. (a): Amplitude of wave envelope ψ of the cnoidal-wave solution for $\kappa = 0.8$, including the (ξ, T)-location of the poles (red). (b) Behavior of the amplitude of the corresponding auxiliary variable $\widetilde{\psi}$ of the cnoidal-wave solution for $\kappa = 0.2$ at $r = 0$ against s. (c) Behavior of the amplitude of the corresponding auxiliary variable $\widetilde{\psi}$ of the cnoidal-wave solution for $\kappa = 0.8$ at $r = 0$ against s. (d): s-coordinate of the corresponding first three poles below the still water surface against the elliptic modulus κ.

which are located below the still water surface at $s = 0$, are highlighted by red lines. It can be seen that the s-coordinates of the poles of $\widetilde{\psi}$ depend on κ. Fig. 4d shows the s-coordinates of the first three poles, which are located below the still water surface at $s = 0$, against κ. It can be seen that the corresponding s-coordinates increase with increasing κ. This indicates that the velocity potential ϕ can be computed without any poles for larger depths if κ is large. However, for all $\kappa \in (0, 1]$, it is found that the velocity potential ϕ corresponding to the cnoidal-wave solution of the NLS (13) can only be computed without any singularity for depths

$$z = \frac{Z}{\varepsilon} > z_{\mathrm{CN}} := -\frac{1}{\varepsilon \psi_0 b} \kappa K'(\kappa) = -\frac{1}{\sqrt{2} \varepsilon \psi_0 k_0^2} \kappa K'(\kappa). \tag{32}$$

3.4. Two-soliton solution

By using the Darboux transformation (Akhmediev and Ankiewicz, 1997) or dressing method (Zakharov and Gelash, 2013), multi-soliton solutions of the NLS can be constructed. The two-soliton solution describes the attraction and interaction of two solitons with equal amplitude. Outside the single impact location, the two pulses diverge from each other. The two-soliton solution has originally been stated in Akhmediev and Ankiewicz (1993). Applied on the NLS (13) with coefficients ν, δ and c_{gr}, the two-soliton solution is given by

$$\psi(X,T) = 8\mathrm{i}\psi_0 \frac{\begin{array}{r} 2b\psi_0\left(X-c_{\mathrm{gr}}T\right)\sinh\left(2b\psi_0\left(X-c_{\mathrm{gr}}T\right)\right) \\ -\left(1-4\mathrm{i}\delta\psi_0^2T\right)\cosh\left(2b\psi_0\left(X-c_{\mathrm{gr}}T\right)\right)\end{array}}{\cosh\left(4b\psi_0\left(X-c_{\mathrm{gr}}T\right)\right)+1+8b^2\psi_0^2\left(X-c_{\mathrm{gr}}T\right)^2+32\delta^2\psi_0^4T^2} \mathrm{e}^{-2\mathrm{i}\delta\psi_0^2T}, \tag{33}$$

whereby b is given by Eq. (20). Figs. 5a-5b show the amplitude of the two-soliton solution for $k_0 = 0.5\,\mathrm{m}^{-1}$, $\psi_0 = 1\,\mathrm{m}$, and $\varepsilon = 0.1$ with respect to the moving coordinate $\xi = X - c_{\mathrm{gr}}T$ from two different perspectives. It can be seen that both solitons interact at $(\xi, T) \approx (0, 0)$ and diverge before and after this point.

In terms of the dimensionless coordinates r, s and τ, the corresponding auxiliary variable $\widetilde{\psi}$ is given by

$$\widetilde{\psi}(X,Z,T) = 8\mathrm{i}\psi_0 \frac{2(r-\mathrm{i}s)\sinh(2(r-\mathrm{i}s)) - (1-4\mathrm{i}\tau)\cosh(2(r-\mathrm{i}s))}{\cosh(4(r-\mathrm{i}s))+1+8(r-\mathrm{i}s)^2+32\tau^2}\mathrm{e}^{-2\mathrm{i}\tau}. \tag{34}$$

As $\cosh(\cdot)$ and $\sinh(\cdot)$ do not contain any poles in the complex plane, also the numerator of $\widetilde{\psi}$ does not contain any poles. The question is whether and where the denominator of $\widetilde{\psi}$ becomes zero. Using hyperbolic trigonometric identities, the denominator of $\widetilde{\psi}$ becomes

$$\begin{aligned} &\cosh(4(r-\mathrm{i}s))+1+8(r-\mathrm{i}s)^2+32\tau^2 \\ &= \underbrace{\left[\cos(4s)\cosh(4r)+1+8r^2-8s^2+32\tau^2\right]}_{=(*)} - \mathrm{i}\underbrace{\left[\sin(4s)\sinh(4r)+16rs\right]}_{=(**)}. \end{aligned} \tag{35}$$

The whole term vanishes for $(*) = 0$ and $(**) = 0$. For $s \neq 0$, the equation $(**) = 0$ has always the root $r = 0$. Furthermore, if $\sin(2s)/s < 0$, the equation $(**) = 0$ has two more roots $r = \pm\bar{r}$. However, the value of $\bar{r}$ can only be computed numerically by solving $(**) = 0$ using, for example, the Newton-Raphson scheme.

For $r = 0$, solving equation $(*) = 0$ yields the solutions $s = \pm\bar{s}_1$. For $r \neq 0$, both equations $(*) = 0$ and $(**) = 0$ must be fulfilled by solving a system of nonlinear equations. This yields the corresponding solutions $r = \pm\bar{r}$ and $s = \pm\bar{s}_2$. Thus, the nonlinear system of equations $(*) = 0$ and $(**) = 0$ has the six solutions $(r, s) = \{(0, \bar{s}_1), (0, -\bar{s}_1), (\bar{r}, \bar{s}_2), (\bar{r}, -\bar{s}_2), (-\bar{r}, \bar{s}_2), (-\bar{r}, -\bar{s}_2)\}$. Note that, as the equation $(**) = 0$ involves the normalized time τ, all six solutions are time-dependent.

The (ξ, T)-coordinates of the poles are highlighted in red in Figs. 5a-5b. It can be seen that one pole is located at $\xi = 0$ for all times. Outside the time period during which the two soliton solutions interact, it is observed that poles are located directly below the positions where the wave envelope ψ of the two single solitons has its maximal amplitude.

Fig. 5c depicts the s-coordinate of the poles of $\widetilde{\psi}$ by showing the values of $-\bar{s}_1 < 0$ and $-\bar{s}_2 < 0$ against the normalized time τ. It can be seen that the maximum of both $-\bar{s}_1$ and $-\bar{s}_2$ over the normalized time τ occurs at $\tau = 0$ and is given by $-\bar{s}_1(\tau = 0) = -0.3695$. By transforming the coordinate s back to Z, it is found that the velocity potential $\phi(x, z, t)$ corresponding to the two-soliton solution of the NLS (13) can be computed without any singularity only for depths

$$z = \frac{Z}{\varepsilon} > z_{\mathrm{TS}} := -\frac{0.3695}{\varepsilon\psi_0 b} = -\frac{0.3695}{\sqrt{2}\varepsilon\psi_0 k_0^2}. \tag{36}$$

3.5. Satsuma-Yajima breather

Besides the two-soliton solution, the Satsuma-Yajima breather solution describes the dynamics of two solitons located at the same spatial position, with fixed but different amplitudes and zero velocities. The Satsuma-Yajima breather solution has originally been derived in Satsuma and Yajima (1974). Applied on the NLS (13) with coefficients ν, δ and c_{gr}, the Satsuma-Yajima breather solution is given by

$$\begin{aligned} &\psi(X,T) = \\ &4\psi_0 \frac{\cosh\left(3b\psi_0\left(X-c_{\mathrm{gr}}T\right)\right)+3\cosh\left(b\psi_0\left(X-c_{\mathrm{gr}}T\right)\right)\exp\left(-4\mathrm{i}\delta\psi_0^2T\right)}{\cosh\left(4b\psi_0\left(X-c_{\mathrm{gr}}T\right)\right)+4\cosh\left(2b\psi_0\left(X-c_{\mathrm{gr}}T\right)\right)+3\cos\left(-4\delta\psi_0^2T\right)} \\ &\mathrm{e}^{-\frac{1}{2}\mathrm{i}\delta\psi_0^2T}. \end{aligned} \tag{37}$$

Fig. 6a shows the amplitude of the Satsuma-Yajima breather for $k_0 = 0.5\,\mathrm{m}^{-1}$, $\psi_0 = 1\,\mathrm{m}$, and $\varepsilon = 0.1$ with respect to the moving coordinate $\xi = X - c_{\mathrm{gr}}T$. It can be seen that the solution beats with a specified frequency in time. For $|\xi| \to \infty$, this solution tends to zero.

When investigating the singularity of the corresponding auxiliary variable $\widetilde{\psi}$ in water depth, it has to be checked again whether and where the denominator of the auxiliary variable $\widetilde{\psi}$ becomes zero. In this way, in terms of the dimensionless coordinates r, s, and τ, algebraic calculations reveal that $\widetilde{\psi}$ becomes singular at $r = 0$ for all $\tau \in \mathbb{R}$. The corresponding s-coordinate satisfies

$$\begin{aligned} \cos(2s) = -1 + \sqrt{\frac{3}{2}}\sqrt{1-\cos(4\tau)} &\Leftrightarrow s \\ &= \pm\frac{1}{2}\cos^{-1}\left(-1 + \sqrt{\frac{3}{2}}\sqrt{1-\cos(4\tau)}\right) + n\pi, \text{ with } n \in \mathbb{Z}. \end{aligned} \tag{38}$$

For completeness, it is noted that another root of the denominator of $\widetilde{\psi}$ is located at $r = 0$, $2s = (2m + 1)\pi$, and $\tau = \pm\frac{1}{2}n\pi$ with $m, n \in \mathbb{Z}$. However, for this combination of r, s, and τ, it can be calculated that the numerator of $\widetilde{\psi}$ is also zero. Convergence analysis reveal that $\widetilde{\psi}$ has no poles at this combination of r, s, and τ.

Fig. 6a highlights the (ξ, T)-coordinates of the pole given at $r = \xi = 0$ in red. It can be seen that the pole is located directly below the position where the wave envelope ψ has its maximal amplitude in space.

From Eq. (38), it results that $\widetilde{\psi}$ contains infinitely many poles in s-direction that behave periodically in τ. Fig. 6b shows the s-coordinate of the first six poles against the normalized time τ. It can be seen that the maximal value of the s-coordinate of the poles occurs at $\tau = \frac{\pi}{4} + m\frac{\pi}{2}$, $m \in \mathbb{Z}$, with $s = -\frac{1}{2}\cos^{-1}(\sqrt{3} - 1) \approx -0.3747$. Therefore, by transforming the coordinate s back to Z, it is found that the velocity potential $\phi(x, z, t)$ corresponding to the Satsuma-Yajima breather solution of the NLS (13) can be computed without any singularity only for depths

$$z = \frac{Z}{\varepsilon} > z_{\mathrm{SY}} := -\frac{\cos^{-1}(\sqrt{3}-1)}{2\varepsilon\psi_0 b} \approx -\frac{0.3747}{\sqrt{2}\varepsilon\psi_0 k_0^2}. \tag{39}$$

3.6. Peregrine breather solution

An important analytical solution of the NLS, which is localized in time and space, has been found by Peregrine (1983) and is known as the Peregrine breather solution. Applied on the NLS (13) with coefficients ν, δ and c_{gr}, this solution is given by

$$\psi(X,T) = \psi_0\left(\frac{4\nu\left(1-2\mathrm{i}\delta\psi_0^2T\right)}{\nu\left[1+\left(2\delta\psi_0^2T\right)^2\right]+2\delta\psi_0^2\left(X-c_{\mathrm{gr}}T\right)^2} - 1\right)\mathrm{e}^{-\mathrm{i}\delta\psi_0^2T}. \tag{40}$$

Fig. 7 shows the amplitude $|\psi|$ of the Peregrine breather solution for $\psi_0 = 1\,\mathrm{m}$, $k_0 = 0.5\,\mathrm{m}^{-1}$, and $\varepsilon = 0.1$. It is clearly shown that the Peregrine breather solution is doubly localized. Therefore, the Peregrine breather solution describes a unique wave event in which large amplitude waves seem to come out of nowhere and disappear without a trace (Chabchoub et al., 2012).

In order to check if the corresponding auxiliary variable $\widetilde{\psi}$ contains singularities, it has to be investigated whether and where the corresponding denominator of $\widetilde{\psi}$ becomes zero. In this way, in terms of the

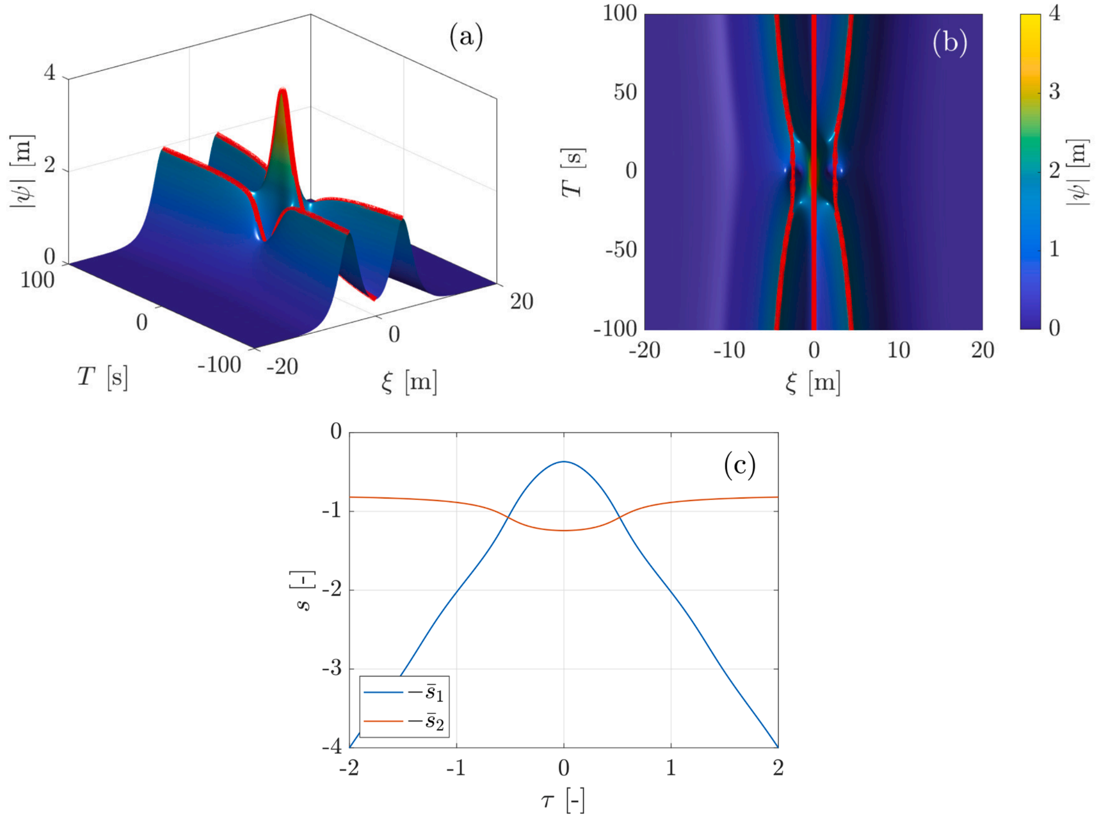

Fig. 5. (a)-(b): Amplitude of wave envelope ψ of the two-soliton solution including the (ξ, T)-location of the poles (red). The value of $|\psi|$ is shown from two different perspectives. (c): s-coordinate of the poles $-\bar{s}_1$ and $-\bar{s}_2$ against the normalized time τ.

dimensionless coordinates r, s and τ, algebraic calculations reveal that $\tilde{\psi}$ becomes singular at

$$r = 0 \quad \text{and} \quad s = \pm\frac{1}{2}\sqrt{1+4\tau^2}. \tag{41}$$

The (ξ, T)-coordinate of the pole is highlighted in red in Fig. 7. It can be seen that the pole is located below the position where the associated wave envelope ψ has its maximum in space.

Considering only the negative values of s, since these are located below the still water surface, it follows from Eq. (41) that the Peregrine breather solution contains poles with s-coordinate $s \leq -\frac{1}{2}$. Consequently, the velocity potential $\phi(x, z, t)$ corresponding to the Peregrine breather solution of the NLS (13) can be computed without any singularity only for depths

$$z = \frac{Z}{\varepsilon} > z_{\mathrm{PB}} := -\frac{1}{2\varepsilon\psi_0 b} = -\frac{1}{2\sqrt{2}\varepsilon\psi_0 k_0^2}. \tag{42}$$

3.7. Time-periodic Kuznetsov-Ma breather

Kuznetsov (1977), Ma (1979) have found a family of time-periodic breather solutions. Applied on the NLS (13) with coefficients ν, δ and c_{gr}, the family of Kuznetsov-Ma breather solutions is given by

$$\psi(X,T) = \psi_0 \frac{\cos\left(0.5\Omega\delta\psi_0^2 T + 2\mathrm{i}\varphi\right) - \cosh(\varphi)\cosh\left(pb\psi_0\left(X - c_{\mathrm{gr}}T\right)\right)}{\cos\left(0.5\Omega\delta\psi_0^2 T\right) - \cosh(\varphi)\cosh\left(pb\psi_0\left(X - c_{\mathrm{gr}}T\right)\right)} \mathrm{e}^{-\mathrm{i}\delta\psi_0^2 T}, \tag{43}$$

with

$$\varphi \in \mathbb{R}, \quad p = 2\sinh(\varphi), \quad \Omega = 2\sinh(2\varphi) \tag{44}$$

and b from Eq. (20). Fig. 8a shows the amplitude $|\psi|$ of the Kuznetsov-Ma breather solution for $\psi_0 = 1\,\mathrm{m}$, $k_0 = 0.5\,\mathrm{m}^{-1}$, $\varepsilon = 0.1$, and $\varphi = 1$. It can be clearly seen that the Kuznetsov-Ma breather solution is periodic in time. Note that the Peregrine breather solution from Eq. (40) can be understood as a limiting case of the Kuznetsov-Ma breather solution when $\varphi \to 0$, i. e. when the breathing period of the solution becomes infinite (Chabchoub, 2013). Therefore, in the following, the Kuznetsov-Ma breather solution is always considered for $\varphi \neq 0$.

In order to check if the corresponding auxiliary variable $\tilde{\psi}$ contains any singularity under water, it has to be investigated whether and where the corresponding denominator of $\tilde{\psi}$ becomes zero. In this way, in terms of the dimensionless coordinates r, s and τ, algebraic calculations reveal that the auxiliary variable $\tilde{\psi}$ becomes singular for

$$r = 0 \quad \text{and} \quad \cos(ps) = \frac{\cos(0.5\Omega\tau)}{\cosh(\varphi)} \Leftrightarrow s = \pm\frac{1}{p}\cos^{-1}\left(\frac{\cos(0.5\Omega\tau)}{\cosh(\varphi)}\right) + 2n\pi, \ \text{with } n \in \mathbb{Z}. \tag{45}$$

As the pole is located at $r = 0$, it is also directly below the point where the wave envelope ψ has its maximal amplitude in space. This is also shown in Fig. 8a, where the (ξ, T)-coordinate of the pole is highlighted in red.

Considering Eq. (45), it can be seen that $\tilde{\psi}$ contains infinitely many poles in s-direction, which behave periodically in τ. Fig. 8b shows the s-coordinate of the first five poles below the still water level against the normalized time τ for $\varphi = 1$. It can be seen that the maximal value of the s-coordinate of the poles below zero, which is denoted by $s_{\max}$, is reached at $\tau = \frac{4m\pi}{\Omega}$, $m \in \mathbb{Z}$, with

$$s_{\max} = -\left|\frac{1}{p}\cos^{-1}\left(\frac{1}{\cosh(\varphi)}\right)\right| \quad \text{for all } \varphi \in \mathbb{R}. \tag{46}$$

Note that $s_{\max}$ depends on φ. Fig. 8c shows the value of $s_{\max}$ against φ. It can be seen that for large $|\varphi|$, the auxiliary variable $\tilde{\psi}$ can be computed free of singularities only down to very small water depths Z. On the

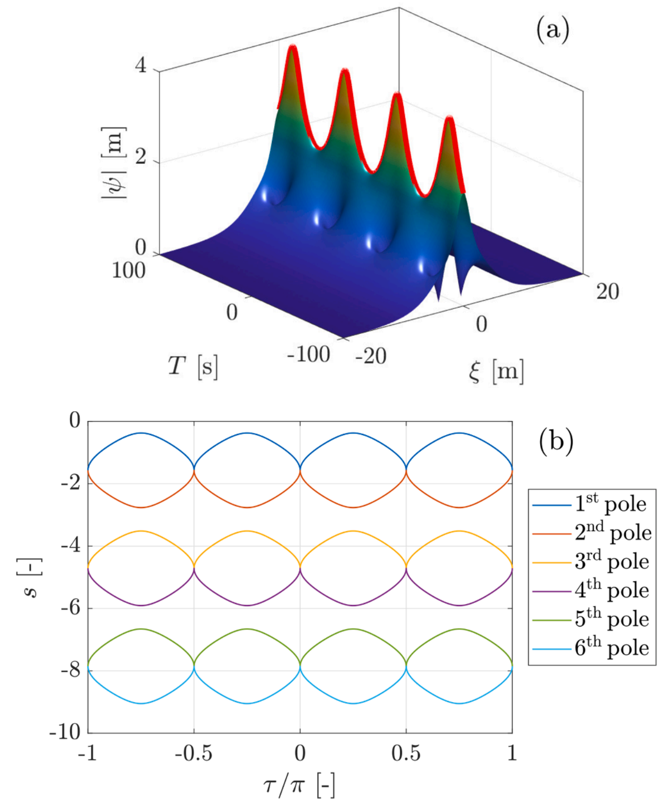

Fig. 6. (a): Amplitude of wave envelope ψ of the Satsuma-Yajima breather including the (ξ, T)-location of the poles (red). (b): s-coordinate of first six poles below $s < 0$ against the normalized time τ.

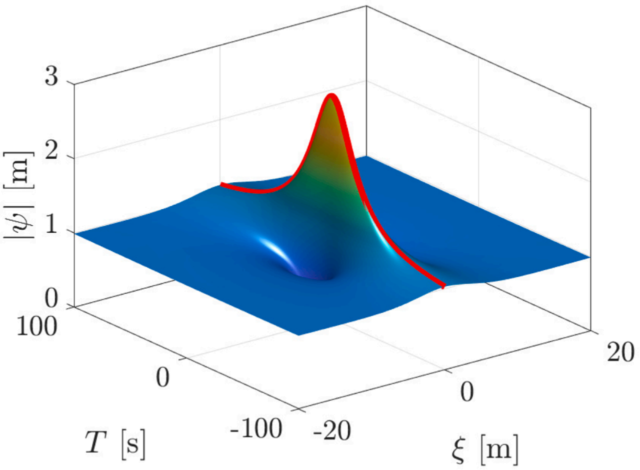

Fig. 7. Amplitude of wave envelope ψ of the Peregrine breather solution including the (ξ, T)-location of the poles (red).

other side, for $|\varphi| \to 0$, the value of $s_{\max}$ decreases monotonically and converges to $s_{\max} = -\frac{1}{2}$.

By transforming the coordinate s back to Z, it results that the velocity potential $\phi(x, z, t)$ corresponding to the Kuznetsov-Ma breather solution of the NLS (13) can be computed without any singularity only for depths

$$z = \frac{Z}{\varepsilon} > z_{\mathrm{KM}} := \frac{s_{\max}}{\varepsilon b \psi_0} = -\left| \frac{\cos^{-1}\left(\frac{1}{\cosh(\varphi)}\right)}{\varepsilon p b \psi_0} \right| \geq -\frac{1}{2\varepsilon b \psi_0} = -\frac{1}{2\sqrt{2}\varepsilon \psi_0 k_0^2} = z_{\mathrm{PB}}. \tag{47}$$

whereby z_{PB} is given by Eq. (42). In terms of the depth z, down to which the velocity potential $\phi(x, z, t)$ can be computed without containing any singularity, it follows that the singularity of the Peregrine breather solution can be understood as a lower bound for the singularity of the Kuznetsov-Ma breather solution for all $\varphi \in \mathbb{R}$.

3.8. Space-periodic Akhmediev breather

Akhmediev (Akhmediev et al., 1985; Akhmediev and Korneev, 1986) proved the existence of a family of space-periodic breather solutions. Applied on the NLS (13) with coefficients ν, δ and c_{gr}, the family of Akhmediev breather solutions is given by

$$\psi(X, T) = \psi_0 \frac{\cosh\left(0.5\Omega\delta\psi_0^2 T + 2\mathrm{i}\varphi\right) - \cos(\varphi)\cos\left(p b \psi_0 \left(X - c_{\mathrm{gr}} T\right)\right)}{\cosh\left(0.5\Omega\delta\psi_0^2 T\right) - \cos(\varphi)\cos\left(p b \psi_0 \left(X - c_{\mathrm{gr}} T\right)\right)} \mathrm{e}^{-\mathrm{i}\delta\psi_0^2 T}, \tag{48}$$

with

$$\varphi \in \mathbb{R}, \quad p = 2\sin(\varphi), \quad \Omega = 2\sin(2\varphi) \tag{49}$$

and b from Eq. (20). Fig. 9a shows the amplitude $|\psi|$ of the Akhmediev breather solution for $\psi_0 = 1\,\mathrm{m}$, $k_0 = 0.5\,\mathrm{m}^{-1}$, $\varepsilon = 0.1$, and $\varphi = 1$. It can be clearly seen that the Akhmediev is periodic in space. As it has also been the case for the Kuznetsov-Ma breather solution from (43), the Peregrine breather solution from Eq. (40) can be understood as a limiting case of the Akhmediev breather solution when $\varphi \to 0$. Therefore, in the following, the Akhmediev breather solution is always considered for $\varphi \neq 0$.

Before investigating the auxiliary variable $\widetilde{\psi}$ corresponding to the Akhmediev breather solution for singularities, it should first be noted that when $\cos(\varphi) = 0$, it follows $\Omega = 0$ and $\psi(X, T) = -\psi_0 \mathrm{e}^{-\mathrm{i}\delta\psi_0^2 T}$. This is the negative of the plane-wave solution from Eq. (22) with $k_{\mathrm{pw}} = 0$. So for $\cos(\varphi) = 0$, the Akhmediev breather solution does not contain any singularity under water.

Again, to check whether the corresponding auxiliary variable $\widetilde{\psi}$ has singularities, it has to be investigated whether and where the denominator of $\widetilde{\psi}$ becomes zero. In this way, in terms of the dimensionless coordinates r, s and τ, algebraic calculations reveal that the auxiliary variable $\widetilde{\psi}$ becomes singular for

- $\cos(\varphi) > 0 \;\Rightarrow\;$ singularity is located at $r = 2m\pi/p$, $m \in \mathbb{Z}$, and $\cosh(ps) = \frac{\cosh(0.5\Omega\tau)}{\cos(\varphi)}$,
- $\cos(\varphi) < 0 \Rightarrow$ singularity is located at $r = (2m+1)\pi/p$, $m \in \mathbb{Z}$, and $\cosh(ps) = \frac{\cosh(0.5\Omega\tau)}{-\cos(\varphi)}$.

It is observed that $\widetilde{\psi}$ contains poles periodically in r. This can also be seen in Fig. 9, where the (ξ, T)-coordinate of the poles is highlighted in red.

Furthermore, it is observed that, independent of the sign of $\cos(\varphi)$, the s-coordinate of the pole is given by

$$\cosh(ps) = \frac{\cosh(0.5\Omega\tau)}{|\cos(\varphi)|} \Leftrightarrow s = \pm\frac{1}{p}\cosh^{-1}\left(\frac{\cosh(0.5\Omega\tau)}{|\cos(\varphi)|}\right). \tag{50}$$

It can be seen that the s-coordinate of the poles depends on τ and φ. Over time, the maximum value of the pole below the still water surface occurs at $\tau = 0$ and is given by

$$s_{\max} = -\left|\frac{1}{p}\cosh^{-1}\left(\frac{1}{|\cos(\varphi)|}\right)\right|. \tag{51}$$

Fig. 9b shows the dependency of $s_{\max}$ on φ. As already discussed, if $\cos(\varphi) \to 0$, the Akhmediev breather solution tends to the plane-wave solution, which does not contain any poles. This can also be seen in Fig. 9b, as $s_{\max} \to -\infty$ for $\varphi \to \frac{1}{2}(2m+1)\pi$, $m \in \mathbb{Z}$. On the other side, the value of $s_{\max}$ can increase up to $s_{\max} = -\frac{1}{2}$, which is also the maximal value for the s-coordinate that has been found in Sec. 3.6 for the Peregrine breather solution, see Eq. (41) for $\tau = 0$.

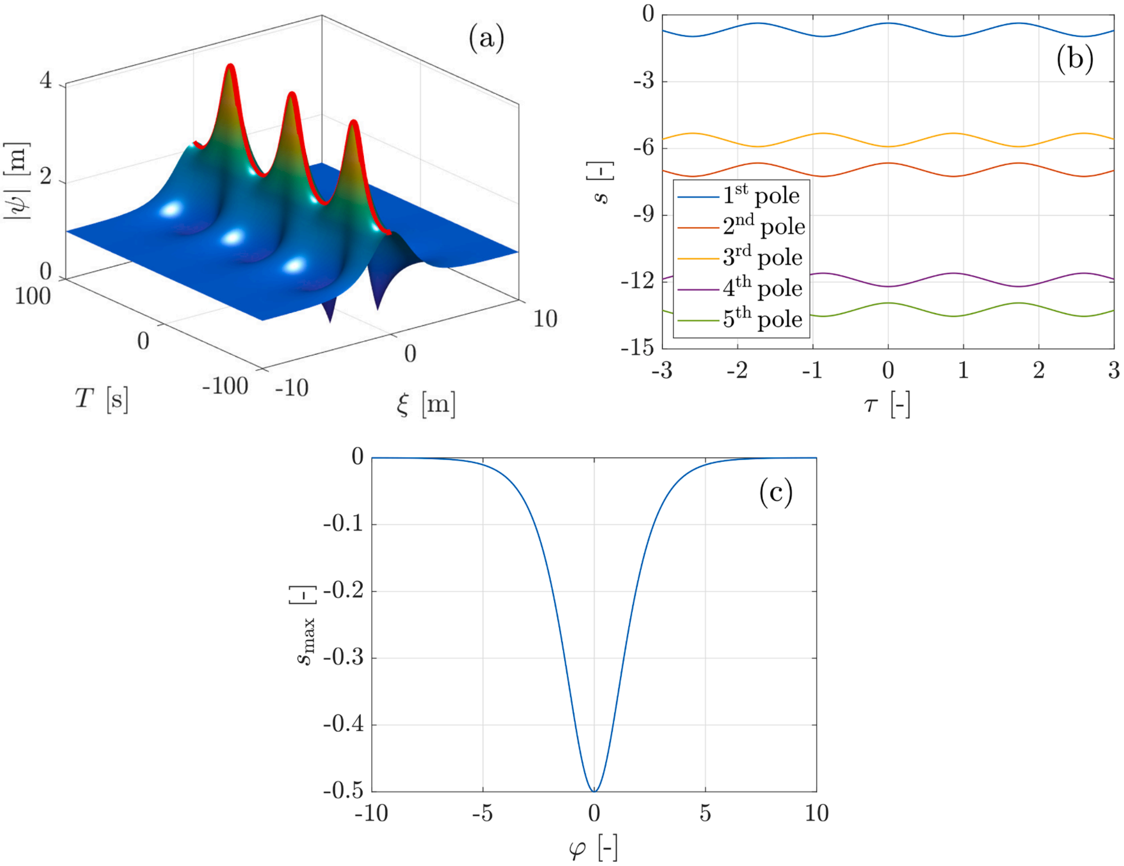

Fig. 8. (a): Amplitude of wave envelope ψ of the Kuznetsov-Ma breather solution including the (ξ, T)-location of the poles (red). (b): s-coordinate of first five poles below $s < 0$ against the normalized time τ. (c): Value of $s_{\max}$ against φ.

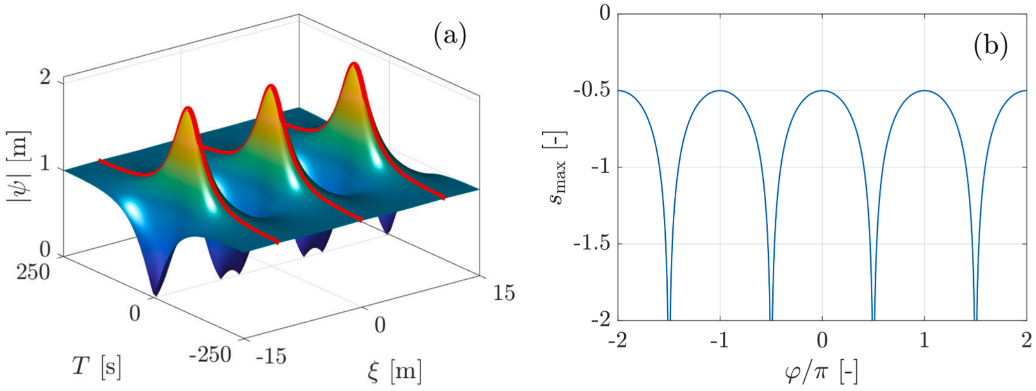

Fig. 9. (a): Amplitude of wave envelope ψ of the Akhkmediev breather solution including the (ξ, T)-location of the poles (red). (b): Value of $s_{\max}$ against φ.

Therefore, by transforming the coordinate s back to Z, it is found that the velocity potential $\phi(x, z, t)$ corresponding to the Akhmediev breather solution of the NLS (13) can be computed without any singularity only for depths

$$z = \frac{Z}{\varepsilon} > z_{\mathrm{AB}} := \frac{s_{\max}}{\varepsilon b \psi_0} = -\left|\frac{\cosh^{-1}\left(\frac{1}{|\cos(\varphi)|}\right)}{\varepsilon p b \psi_0}\right| = -\left|\frac{\cosh^{-1}\left(\frac{1}{|\cos(\varphi)|}\right)}{2\sqrt{2}\sin(\varphi)\varepsilon k_0^2 \psi_0}\right|. \tag{52}$$

Since $s_{\max} \le -\frac{1}{2}$, it also follows $z_{\mathrm{AB}} \le -\frac{1}{2\varepsilon b \psi_0} = -\frac{1}{2\sqrt{2}\varepsilon \psi_0 k_0^2} = z_{\mathrm{PB}}$ for all $\varphi \in \mathbb{R}$, whereby z_{PB} is given by Eq. (42). In terms of the depth z, down to which the velocity potential $\phi(x, z, t)$ can be computed without containing any singularity, it follows that the singularity of the Peregrine breather solution can be understood as an upper bound for the singularity of the Akhmediev breather solution for all $\varphi \in \mathbb{R}$.

Finally, note that for $\varphi \to (2m+1)\pi$, $m \in \mathbb{Z}$, $s_{\max}$ converges to $s_{\max} \to -\frac{1}{2}$. Nevertheless, the auxiliary variable $\widetilde{\psi}$ does not contain any singularities in space, since the denominator of $\widetilde{\psi}$ becomes zero only at $r = (2m+1)\pi/p \to \pm\infty$, $m \in \mathbb{Z}$. Therefore, the auxiliary variable $\widetilde{\psi}$ corresponding to the Akhmediev breather solutions does not contain any singularity in water depth for $\varphi = \frac{1}{2}(2m+1)\pi$ and $\varphi = (2m+1)\pi$, $m \in \mathbb{Z}$. For all other values of φ, $\widetilde{\psi}$ contains singularities, and the corresponding velocity potential ϕ can be computed without any singularity down to the water depth $z = z_{\mathrm{AB}}$ from Eq. (52).

3.9. Rational localized solutions of the NLS

The Peregrine solution of the NLS (13) is not the only one that is localized in time and space. It has been found that the NLS has a whole hierarchy of breather solutions localized in time and space, see e.g. Akhmediev et al. (2009). The j-th order rational solution of the NLS, also known as the j-th Akhmediev-Peregrine solution, can be written in the general form

$$\psi(X,T)=\psi_0\left[(-1)^j+\frac{G_j+\mathrm{i}H_j}{D_j}\right]\mathrm{e}^{-\mathrm{i}\delta\psi_0^2T} \tag{53}$$

with some polynomials $G_j(X,T)$, $H_j(X,T)$ and $D_j(X,T)$. For the first seven orders, the corresponding functions G_j, H_j and D_j are given in Akhmediev et al. (2009), Gaillard (2013). In particular, for $j=1$ and applied on the NLS (13) with coefficients ν, δ and c_{gr}, the Peregrine breather solution from Eq. (40) results with

$$G_1(X,T)=4\nu, \tag{54a}$$

$$H_1(X,T)=-8\nu\delta\psi_0^2T, \tag{54b}$$

$$D_1(X,T)=\nu\left[1+\left(2\delta\psi_0^2T\right)^2\right]+2\delta\psi_0^2\left(X-c_{\mathrm{gr}}T\right)^2. \tag{54c}$$

For $j=2$, the corresponding polynomials G_2, H_2 and D_2 for the NLS (13) are given by

$$\begin{aligned}G_2(X,T)=&\frac{3}{4}-\left(b^2\psi_0^2\left(X-c_{\mathrm{gr}}T\right)^2+\delta^2\psi_0^4T^2+3/4\right)\\&\left(b^2\psi_0^2\left(X-c_{\mathrm{gr}}T\right)^2+5\delta^2\psi_0^4T^2+3/4\right),\end{aligned} \tag{55a}$$

$$\begin{aligned}H_2(X,T)=&\delta\psi_0^2T\left[\delta^2\psi_0^4T^2-3b^2\psi_0^2\left(X-c_{\mathrm{gr}}T\right)^2\right.\\&\left.+2\left[b^2\psi_0^2\left(X-c_{\mathrm{gr}}T\right)^2+\delta^2\psi_0^4T^2\right]^2-\frac{15}{8}\right],\end{aligned} \tag{55b}$$

$$\begin{aligned}D_2(X,T)=&\frac{1}{3}\left[b^2\psi_0^2\left(X-c_{\mathrm{gr}}T\right)^2+\delta^2\psi_0^4T^2\right]^3\\&+\frac{1}{4}\left[b^2\psi_0^2\left(X-c_{\mathrm{gr}}T\right)^2-3\delta^2\psi_0^4T^2\right]^2\\&+\frac{3}{64}\left[12b^2\psi_0^2\left(X-c_{\mathrm{gr}}T\right)^2+44\delta^2\psi_0^4T^2+1\right].\end{aligned} \tag{55c}$$

Corresponding expressions for higher-order solutions are progressively more complicated. In the following, only the second-order solution is considered. Figs. 10a-10b show the amplitude $|\psi|$ of the 2-nd Akhmediev-Peregrine solution for $\psi_0=1\,\mathrm{m}$, $k_0=0.5\,\mathrm{m}^{-1}$, and $\varepsilon=0.1$ from two different perspectives. This solution can be seen as a single splash with a high amplitude in the middle and constant amplitude outside of the splash.

In order to check if the corresponding auxiliary variable $\widetilde{\psi}$ has poles, it has to be investigated whether and where the denominator of $\widetilde{\psi}$ becomes zero. Therefore, it has to be analyzed for which (X,Z,T) the condition $D_2(X-\mathrm{i}Z,T)=0$ is satisfied. In terms of the dimensionless coordinates r, s and τ, algebraic calculations reveal that the imaginary part of $D_2(X-\mathrm{i}Z,T)$ vanishes if $r=0$ or if r, s, and τ satisfy

$$2(r^2+\tau^2-s^2)^2+(r^2-3\tau^2-s^2)-\frac{8}{3}r^2s^2+\frac{9}{8}=0. \tag{56}$$

In the first case, for $r=0$, it has to be checked for which s the real part of the function $D_2(X-\mathrm{i}Z,T)$ vanishes. Here, a polynomial of 3-rd order in s^2 has to be solved for s. Analyzing all roots, it can be seen that only one root for s^2 is real-valued for all $\tau\in\mathbb{R}$. Defining

$$d=\sqrt[3]{\sqrt{2304\tau^8+1792\tau^6+864\tau^4-144\tau^2+9}+48\tau^4+24\tau^2-1}>0, \tag{57}$$

the corresponding s-coordinate of the root of $D_2(X-\mathrm{i}Z,T)$ is given by

$$s=\pm\sqrt{\tau^2+\frac{d}{2}+\frac{4\tau^2-1}{d}+\frac{1}{4}}. \tag{58}$$

In the second case, for $r\neq 0$, it has to be checked for which (r,s,τ) Eq. (56) is fulfilled and the real part of $D_2(X-\mathrm{i}Z,T)$ vanishes. This leads to a system of polynomials of third order in r^2 and s^2. A further analysis of all roots shows that for each of s^2 and r^2, only one root is real-valued for all $\tau\in\mathbb{R}$. Using d from Eq. (57) and defining

$$u=-\tau^2+\frac{d}{4}+\frac{4\tau^2-1}{2d}-\frac{1}{4}, \tag{59}$$

$$w=-\frac{u}{2}+\frac{1}{2}\sqrt{\frac{\begin{array}{l}64\tau^6+192\tau^4u+432\tau^4+384\tau^2u^2-288\tau^2u\\+396\tau^2+256u^3+96u^2+108u+9\end{array}}{48(4\tau^2+4u+1)}}, \tag{60}$$

it is found that the corresponding r- and s-coordinates of the roots of $D_2(X-\mathrm{i}Z,T)$ are given by

$$r=\pm\sqrt{u+w},\ \text{and}\ s=\pm\sqrt{w}. \tag{61}$$

Figs. 10a-10b highlights the (ξ,T)-coordinate of the three different poles in red. Furthermore, Fig. 10c shows the s-coordinate of these poles against the normalized time τ. It can be seen that the maximal value of the s-coordinate of the poles is reached at $r=0$ and $\tau=0$ with $s=-\sqrt{\frac{\sqrt[3]{2}}{2}-\frac{1}{\sqrt[3]{2}}+\frac{1}{4}}=\approx-0.2937$.

By transforming the coordinate s back to Z, it is found that the velocity potential $\phi(x,z,t)$ corresponding to the 2-nd Akhmediev-Peregrine solution of the NLS (13) can be computed without any singularity only for depths

$$z=\frac{Z}{\varepsilon}>z_{\mathrm{AP}}:=-\frac{\sqrt{\frac{\sqrt[3]{2}}{2}-\frac{1}{\sqrt[3]{2}}+\frac{1}{4}}}{\varepsilon b\psi_0}\approx-\frac{0.2937}{\sqrt{2}\varepsilon k_0^2\psi_0}. \tag{62}$$

3.10. Pole of auxiliary variable $\widetilde{C}$

Considering Eq. (16), it can be seen that the velocity potential ϕ corresponding to solutions of the NLS depends not only on $\widetilde{\psi}$, but also on the auxiliary variable $\widetilde{C}$. Here, $\widetilde{C}$ is defined by $\widetilde{C}(X,Z,T)=C(X-\mathrm{i}Z,T)$ with $C=|\psi|^2\psi$. To investigate the water depth down to which the velocity potential ϕ can be computed without containing singularities, the singularities of $\widetilde{C}$ also have to be analyzed. However, for all solutions presented so far, it can be found that $\widetilde{C}$ contains singularities at the same locations as $\widetilde{\psi}$:

- For the plane wave solution from Section 3.1, the auxiliary variable $\widetilde{C}$ is given by $\widetilde{C}(X,Z,T)=\psi_0^2\widetilde{\psi}(X,Z,T)$. As $\widetilde{\psi}$ does not contain any singularity in the case of the plane wave solution, neither does $\widetilde{C}$.
- For the soliton and cnoidal-wave solution from Section 3.2 and Section 3.3, the respective auxiliary variable $\widetilde{C}$ is given by

  $$\widetilde{C}(X,Z,T)=\psi_0^2\mathrm{sech}^2\left(\psi_0b\left(X-\mathrm{i}Z-c_{\mathrm{gr}}T\right)\right)\widetilde{\psi}\ \text{ and} \tag{63}$$

  $$\widetilde{C}(X,Z,T)=\psi_0^2\mathrm{cn}^2\left(\frac{\psi_0}{\kappa}b\left(X-\mathrm{i}Z-c_{\mathrm{gr}}T\right),\kappa\right)\widetilde{\psi}. \tag{64}$$

  In both cases, it can be seen that $\widetilde{C}$ contains a singularity at the same location as $\widetilde{\psi}$.
- For all other solutions presented in Section 3.4-3.9, note that the corresponding wave envelope ψ can be written in the general form

  $$\psi(X,T)=\psi_0\frac{F+\mathrm{i}H}{K}\mathrm{e}^{-c\mathrm{i}\delta\psi_0^2T}. \tag{65}$$

  with some real-valued functions $F(X,T)$, $H(X,T)$, and $K(X,T)$ and some real-valued constant c. In this case, the auxiliary variable $\widetilde{C}$ is given by

  $$\widetilde{C}(X,Z,T)=\psi_0^2\frac{F^2(X-\mathrm{i}Z,T)+H^2(X-\mathrm{i}Z,T)}{K^2(X-\mathrm{i}Z,T)}\widetilde{\psi}. \tag{66}$$

  Since the function K appears in Eq. (65) and in Eq. (66), $\widetilde{C}$ contains poles at the same location as $\widetilde{\psi}$.

Therefore, the velocity potential ϕ corresponding to solutions ψ of the NLS can only be computed without singularities down to the depth where $\widetilde{\psi}$ becomes singular.

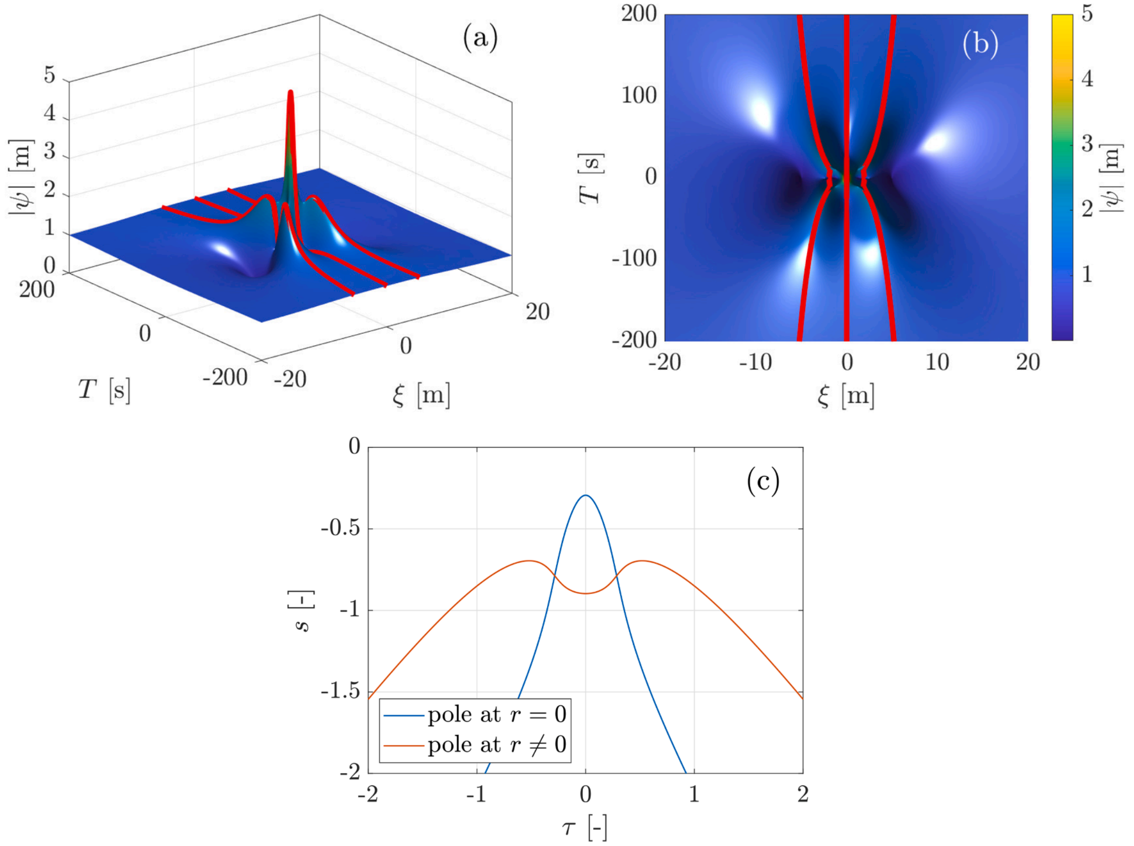

Fig. 10. (a)-(b): Amplitude of wave envelope ψ of the 2-nd Akhmediev-Peregrine solution including the (ξ, T)-location of the poles (red). The value of $|\psi|$ is shown from two different perspectives. (c): s-coordinate of the poles against the normalized time τ.

3.11. Summary and conclusions for fluid dynamics applications

In this section, it has been observed that the velocity potential ϕ corresponding to most of the investigated analytical solutions ψ of the NLS (13) contains singularities at certain water depths. These singularities do not represent a physical divergence of the underlying inviscid potential flow. Instead, they arise as mathematical artifacts caused by the analytic continuation of the wave envelope ψ and auxiliary variable C from the real spatial coordinate X into the complex plane $X - iZ$. In this setting, the functions $\widetilde{\psi}$ and $\widetilde{C}$ arise as the analytic continuations of ψ and C, respectively, and it has been found that $\widetilde{\psi}$ and $\widetilde{C}$ can contain singularities below the still water surface.

Consequently, the velocity potential $\phi(x, z, t)$ corresponding to solutions ψ of the NLS (13) can be computed without any singularity only for small water depths $z_{\text{limit}} < z \leq 0$. Here, the value of z_{limit} depends on the particular analytical solution of the NLS. Table 3.11 summarizes the values of z_{limit}, which have been computed in this section for the investigated analytical solutions of the NLS. It can be seen that the value of z_{limit} can be written in the form $z_{\text{limit}} = -c\gamma$, where $\gamma := \frac{1}{\varepsilon b \psi_0} = \frac{1}{\sqrt{2}\varepsilon\psi_0 k_0^2}$. While γ depends on the amplitude ψ_0, wave steepness ε, and wave number k_0 of the corresponding solution ψ of the NLS, c is constant or depends on the solution-specific parameters κ and φ, respectively.

Considering Tab. 3.11, three different observations can be made: First, it can be observed that the singularity of ϕ can generally appear at every water depth $z < 0$. For example, considering the Akhmediev breather and Kuznetsov-Ma breather solution, it can be observed that $z_{\text{AB}} \in \left(-\infty, -\frac{1}{2\sqrt{2}\varepsilon\psi_0 k_0^2}\right]$ and $z_{\text{KM}} \in \left[-\frac{1}{2\sqrt{2}\varepsilon\psi_0 k_0^2}, 0\right)$, see also Fig. 9 and Fig. 8. Also, considering only the cnoidal solution of the NLS, it can be seen that the singularity of ϕ can generally appear at every water depth $z < 0$. It should be noted that although z_{CN} from Eq. (32) can only take values in the interval $\left[-\frac{\pi}{2\sqrt{2}\varepsilon\psi_0 k_0^2}, 0\right)$, the corresponding singularity appears periodically in z, see Eq. (31).

Second, recall that the NLS is only valid in deep water. Using the wavelength $\lambda = \frac{2\pi}{k_0}$, this means that the water depth $h > 0$ has to satisfy the deep-water condition, $h > \frac{1}{2}\lambda = \frac{\pi}{k_0}$. On the other side, in applications examples like the computation of some fluid-structure interaction in deep water, it has to be ensured that the velocity potential ϕ of the water waves can be computed accurately in the whole computational water domain. When computing the velocity potential ϕ using the NLS, this means that h has to be chosen so that the singularity of ϕ at $z = z_{\text{limit}}$ is located below $-h$, i.e. $-h > z_{\text{limit}}$. It follows that the parameters ψ_0, k_0, ε, κ and φ, on which the different analytical solutions from Sections 3.2-3.9 of the NLS (13) depend, have to satisfy

$$-\frac{\pi}{k_0} > -h > z_{\text{limit}} = -c\gamma = \frac{-c}{\sqrt{2}\varepsilon\psi_0 k_0^2} \Rightarrow \frac{c}{\sqrt{2}\varepsilon\psi_0 k_0} > \pi. \tag{67}$$

For applications like the computation of some fluid-structure interaction, this means that the parameters ψ_0, k_0, ε, κ and φ have to be chosen wisely to satisfy Eq. (67).

Third, recall that the NLS can only be used to accurately model nonlinear water waves with a moderate wave steepness of $\varepsilon \leq 0.15$, see e.g. Dysthe (1979), Osborne (2010), Witt (2019). Because $z_{\text{limit}} = \mathcal{O}(\varepsilon^{-1})$, smaller values of ε generally correspond to larger magnitudes of z_{limit}. However, as has already been observed, even for very small values of ε, the magnitude of z_{limit} can become arbitrarily small.

It can be concluded that although the NLS can be used to accurately model nonlinear water waves in deep water with a narrow spectral band-

Table 1

Overview of several analytical solutions ψ of the NLS and location of the first singularity of the corresponding velocity potential ϕ below the water surface, with $\gamma := \frac{1}{\varepsilon b \psi_0} = \frac{1}{\sqrt{2}\varepsilon \psi_0 k_0^2}$.

Name of analytical solution	Velocity potential $\phi(x, z, t)$ can be computed without containing a singularity for:	Comment
Plane wave solution	$z > -\infty$	no singularity
Soliton solution	$z > z_{\mathrm{Sol}} = -\frac{\pi}{2}\gamma$	periodic singularity in z
Cnoidal-wave solution	$z > z_{\mathrm{CN}} = -\kappa K'(\kappa)\gamma$	periodic singularity in z
Two-soliton solution	$z > z_{\mathrm{TS}} = -0.3695\gamma$	three different singularities in x
Satsuma-Yajima breather solution	$z > z_{\mathrm{SY}} = -\frac{\cos^{-1}(\sqrt{3}-1)}{2}\gamma \approx -0.3747\gamma$	periodic singularity in z and t
Peregrine breather solution	$z > z_{\mathrm{PB}} = -\frac{1}{2}\gamma$	one non-periodic singularity
Kuznetsov-Ma breather solution	$z > z_{\mathrm{KM}} = -\left\lvert \frac{\cos^{-1}\left(\frac{1}{\cosh(\varphi)}\right)}{2\sinh(\varphi)} \right\rvert \gamma$	periodic singularity in z and t, $z_{\mathrm{KM}} \geq z_{\mathrm{PB}}$
Akhmediev breather solution	$z > z_{\mathrm{AB}} := -\left\lvert \frac{\cosh^{-1}\left(\frac{1}{\lvert\cos(\varphi)\rvert}\right)}{2\sin(\varphi)} \right\rvert \gamma$	periodic singularity in x, $z_{\mathrm{AB}} \leq z_{\mathrm{PB}}$
2-nd Akhmediev-Peregrine solution	$z > z_{\mathrm{AP}} := -\sqrt{\frac{\sqrt[3]{2}}{2} - \frac{1}{\sqrt[3]{2}} + \frac{1}{4}}\gamma \approx -0.2937\gamma$	three different singularities in x

width and moderate wave steepness, the corresponding velocity potential $\phi(x, z, t)$ can generally contain unrealistic singularities at every water depth $z < 0$. For solutions such as the soliton solution, where the singularities appear periodically in z, this also means that the condition $\phi_z \to 0$ for $z \to -\infty$ from Eq. (1d) is not fulfilled. In applications, where the velocity potential ϕ corresponding to solutions of the NLS is needed, e.g. the computation of the flow field below the sea surface or some fluid-structure interaction, the wave parameters defining the solutions of the NLS have to be chosen carefully. Here, it has to be ensured that ϕ can be computed accurately throughout the whole water domain considered in numerical simulations, without any singularities occurring.

4. Instability of the numerical method solving the complex transport equation

In the previous section, it has been shown that the auxiliary variables $\widetilde{\psi}(X, Z, T)$ and $\widetilde{C}(X, Z, T)$ can contain singularities in Z. If some closed-form expression for the solution ψ of the NLS (13) is available, the auxiliary variables $\widetilde{\psi}(X, Z, T)$ and $\widetilde{C}(X, Z, T)$ can be calculated by evaluating the variables ψ and $C = |\psi|^2\psi$ at $(X - \mathrm{i}Z, T)$. However, if an analytic expression for ψ is not given but only numerical values of $\psi(X, T)$, the auxiliary variable $\widetilde{\psi}$ can be computed numerically by solving the complex transport equation

$$\widetilde{\psi}_Z = -\mathrm{i}\widetilde{\psi}_X, \quad \text{for } Z < 0, \tag{68a}$$

$$\widetilde{\psi} = \psi, \quad \text{for } Z = 0. \tag{68b}$$

A similar complex transport equation with a different BC at $Z = 0$ can be solved numerically to compute $\widetilde{C}(X, Z, T)$.

In this section, it is investigated how the complex transport Eq. (68) can be solved numerically. Although Eq. (68) is much simpler than the NLS (13), it is shown in this section that the stability of numerical schemes used to solve Eq. (68) is a big issue. In addition to the singularities of $\widetilde{\psi}$ and $\widetilde{C}$ presented in the last section, the instability of numerical schemes used to solve the complex transport Eq. (68) makes it difficult to compute the velocity potential ϕ corresponding to solutions ψ of the NLS accurately in large water depths.

For simplicity, the following refers only to the numerical computation of $\widetilde{\psi}$. The numerical computation of $\widetilde{C}$ follows analogously. Since the complex transport Eq. (68) is defined on an unbounded domain, the $X - Z$-domain must first be bounded, within which the numerical solution is computed, i. e.

$$\begin{aligned} &\widetilde{\psi}_Z = -\mathrm{i}\widetilde{\psi}_X, \quad \text{for } X \in (-X_{\max}, X_{\max}),\ Z \in [Z_{\min}, 0), \\ &\widetilde{\psi}(X, Z = 0) = \psi(X), \quad \text{for } X \in [-X_{\max}, X_{\max}], \\ &\widetilde{\psi}(-X_{\max}, Z) = \widetilde{\psi}(X_{\max}, Z),\ \widetilde{\psi}_X(-X_{\max}, Z) = \widetilde{\psi}_X(X_{\max}, Z) \\ &\text{for } Z \in [Z_{\min}, 0). \end{aligned} \tag{69}$$

Here, the length $X_{\max}$ is assumed to be so large that the basic physical behavior occurs within the range $(-X_{\max}, X_{\max})$. Periodic BCs are applied in X-direction. Furthermore, the value of the water depth $Z_{\min} < 0$ is larger than some $Z_{\mathrm{limit}} < 0$, i. e. $Z_{\mathrm{limit}} < Z_{\min} < 0$. Here, it is assumed that the solution $\widetilde{\psi}$ exists without any singularity down to the depth Z_{limit}. For the analytical solutions presented in Section 3.2-3.9, the value of Z_{limit} is given by $Z_{\mathrm{limit}} = \varepsilon z_{\mathrm{limit}} = \varepsilon c\gamma$ with c and γ as defined in Tab. 3.11.

Next, the domain $[-X_{\max}, X_{\max}] \times [Z_{\min}, 0]$ is discretized using the equidistant grid

$$\begin{aligned} Z_n &:= n\Delta Z, \quad \text{for } n \in \{0, \dots, N\},\ \Delta Z = \frac{Z_{\min}}{N} < 0, \\ X_j &:= j\Delta X - X_{\max}, \quad \text{for } j \in \{0, \dots, J\},\ \Delta X = \frac{2X_{\max}}{J} > 0. \end{aligned} \tag{70}$$

Finally, the grid function P is introduced with $P_j^n = P(X_j, Z_n)$, which serves as an approximation to the exact solution of the complex transport equation at the grid points, i. e. $P_j^n \approx \widetilde{\psi}(X_j, Z_n)$.

The complex transport Eq. (69) is discretized on the grid specified in Eq. (70) by substituting all derivatives with their respective finite difference approximations. Replacing the Z-derivative by a forward and the X-derivative by a central finite difference approximation yield

$$\frac{P_j^{n+1} - P_j^n}{\Delta Z} = -\mathrm{i}\frac{P_{j+1}^n - P_{j-1}^n}{2\Delta X}. \tag{71}$$

This finite-difference scheme has consistency order two in X and consistency order one in Z. However, it is not stable. This is shown below using a von Neumann stability analysis. Details about the von Neumann stability analysis can be found in many standard textbooks, such as Tveito and Winther (1998), Marsal (1976).

Let the numerical approximation error be defined as

$$\beta_j^n := P_j^n - p_j^n. \tag{72}$$

Here, P_j^n represents the solution of Eq. (71) in the absence of any rounding errors, and p_j^n denotes the numerical solution obtained in finite-precision arithmetic. Since both P_j^n and p_j^n satisfy Eq. (71), the numer-

Table 2
Overview of schemes that are frequently used to discretize the general transport equation $\widetilde{\psi}_Z + c\widetilde{\psi}_X = 0$ for an arbitrary constant c. For each scheme, the corresponding computation rule and the amplification factor $|G|^2$ for $c = \mathrm{i}$ with $\theta = \mu_m \Delta X$ are given.

Name of scheme	Computation rule for PDE $\widetilde{\psi}_Z + c\widetilde{\psi}_X = 0$	$\lvert G\rvert^2$ for $c = \mathrm{i}$
Explicit central difference scheme	$P_j^{n+1} = P_j^n - c\frac{\Delta Z}{2\Delta X}\left(P_{j+1}^n - P_{j-1}^n\right)$	$\left(1 + \frac{\Delta Z}{\Delta X}\sin(\theta)\right)^2$
Explicit forward difference scheme	$P_j^{n+1} = P_j^n - c\frac{\Delta Z}{\Delta X}\left(P_{j+1}^n - P_j^n\right)$	$\left(1 + \frac{\Delta Z}{\Delta X}\sin(\theta)\right)^2 + \frac{\Delta Z^2}{\Delta X^2}(1-\cos(\theta))^2$
Explicit backward difference scheme	$P_j^{n+1} = P_j^n - c\frac{\Delta Z}{\Delta X}\left(P_j^n - P_{j-1}^n\right)$	$\left(1 + \frac{\Delta Z}{\Delta X}\sin(\theta)\right)^2 + \frac{\Delta Z^2}{\Delta X^2}(1-\cos(\theta))^2$
Implicit central difference scheme	$P_j^{n+1} = P_j^n - c\frac{\Delta Z}{2\Delta X}\left(P_{j+1}^{n+1} - P_{j-1}^{n+1}\right)$	$1/\left[1 - \frac{\Delta Z}{\Delta X}\sin(\theta)\right]^2$
Implicit forward difference scheme	$P_j^{n+1} = P_j^n - c\frac{\Delta Z}{\Delta X}\left(P_{j+1}^{n+1} - P_j^{n+1}\right)$	$1/\left[\left(1 - \frac{\Delta Z}{\Delta X}\sin(\theta)\right)^2 + \frac{\Delta Z^2}{\Delta X^2}(1-\cos(\theta))^2\right]$
Implicit backward difference scheme	$P_j^{n+1} = P_j^n - c\frac{\Delta Z}{\Delta X}\left(P_j^{n+1} - P_{j-1}^{n+1}\right)$	$1/\left[\left(1 - \frac{\Delta Z}{\Delta X}\sin(\theta)\right)^2 + \frac{\Delta Z^2}{\Delta X^2}(1-\cos(\theta))^2\right]$
Lax-Wendroff scheme	$P_j^{n+1} = P_j^n - c\frac{\Delta Z}{2\Delta X}\left(P_{j+1}^n - P_{j-1}^n\right) + c^2\frac{\Delta Z^2}{2\Delta X^2}\left(P_{j+1}^n - 2P_j^n + P_{j-1}^n\right)$	$\left[1 + \frac{\Delta Z}{\Delta X}\sin(\theta) + \frac{\Delta Z^2}{\Delta X^2}(1-\cos(\theta))\right]^2$
Lax-Friedrichs scheme	$P_j^{n+1} = \frac{1}{2}\left(P_{j+1}^n + P_{j-1}^n\right) - c\frac{\Delta Z}{2\Delta X}\left(P_{j+1}^n - P_{j-1}^n\right)$	$\left[\cos(\theta) + \frac{\Delta Z}{\Delta X}\sin(\theta)\right]^2$
Crank-Nicolson scheme	$P_j^{n+1} = P_j^n - c\frac{\Delta Z}{4\Delta X}\left[\left(P_{j+1}^{n+1} - P_{j-1}^{n+1}\right) + \left(P_{j+1}^n - P_{j-1}^n\right)\right]$	$\left[\left(1 + \frac{\Delta Z}{2\Delta X}\sin(\theta)\right)/\left(1 - \frac{\Delta Z}{2\Delta X}\sin(\theta)\right)\right]^2$
Leapfrog scheme	$P_j^{n+1} = P_j^{n-1} - c\frac{\Delta Z}{\Delta X}\left(P_{j+1}^n - P_{j-1}^n\right)$	$\left[\frac{\Delta Z}{\Delta X}\sin(\theta) \pm \sqrt{\left(\frac{\Delta Z}{\Delta X}\sin(\theta)\right)^2 + 1}\right]^2$

ical error β_j^n also satisfies Eq. (71), i. e.

$$\frac{\beta_j^{n+1} - \beta_j^n}{\Delta Z} = -\mathrm{i}\frac{\beta_{j+1}^n - \beta_{j-1}^n}{2\Delta X}. \tag{73}$$

Since periodic BCs are assumed, β_j^n can be expressed as a truncated Fourier series expansion of the form

$$\beta_j^n = \sum_{m=-J/2}^{J/2-1} \widehat{\beta}_m^n \mathrm{e}^{\mathrm{i}\mu_m X_j}, \quad \text{with } \mu_m = \frac{m\pi}{X_{\max}}. \tag{74}$$

Substituting Eq. (74) into Eq. (73) and considering only the m-th component of the Fourier series results in

$$\frac{\widehat{\beta}_m^{n+1}\mathrm{e}^{\mathrm{i}\mu_m X_j} - \widehat{\beta}_m^n\mathrm{e}^{\mathrm{i}\mu_m X_j}}{\Delta Z} = -\mathrm{i}\frac{\widehat{\beta}_m^n\mathrm{e}^{\mathrm{i}\mu_m X_{j+1}} - \widehat{\beta}_m^n\mathrm{e}^{\mathrm{i}\mu_m X_{j-1}}}{2\Delta X}. \tag{75}$$

Dividing Eq. (75) by $\widehat{\beta}_m^n\mathrm{e}^{\mathrm{i}\mu_m X_j}$ and introducing the amplification factor $G = \widehat{\beta}_m^{n+1}/\widehat{\beta}_m^n$ yields

$$G = 1 - \mathrm{i}\frac{\Delta Z}{2\Delta X}\left(\mathrm{e}^{\mathrm{i}\mu_m\Delta X} - \mathrm{e}^{-\mathrm{i}\mu_m\Delta X}\right) = 1 + \frac{\Delta Z}{\Delta X}\sin(\mu_m\Delta X). \tag{76}$$

The numerical scheme is stable if the error β_j^n does not grow with increasing depth Z. This is the case if $|G| < 1$ for all $\mu_m \in \mathbb{R}$. However, for any given values of ΔZ and ΔX, there exist some μ_m such that $|G| > 1$. Therefore, the finite difference scheme from Eq. (71) is unstable when solving the complex transport Eq. (69).

A natural way to address this problem is to use an alternative scheme to numerically approximate $\widetilde{\psi}$. Table 4 lists several well-known schemes, which are commonly used to discretize the general transport equation $\widetilde{\psi}_Z + c\widetilde{\psi}_X = 0$ for an arbitrary constant c. These schemes can be found, for example, in Langtangen (2003), LeVeque (1992). Table 4 also presents the corresponding computation rule and the amplification factor $|G|$ for $c = \mathrm{i}$. For completeness, the first row summarizes the results for the finite difference scheme from Eq. (71). To simplify the notation, the abbreviation $\theta = \mu_m\Delta X$ is introduced.

To investigate the stability of the schemes listed in Tab. 4 in a better way, Fig. 11 shows the corresponding maximal value of G for $\theta \in [0, 2\pi]$ against $\Delta Z/\Delta X$. Note that the results for the implicit forward, explicit backward, implicit backward, and Leapfrog schemes are not shown in Fig. 11, as they lead to identical or very similar results as the explicit forward scheme. However, Fig. 11 shows that all schemes listed in Tab. 4 yield amplification factors G with $|G| > 1$ for all $\Delta Z/\Delta X \neq 0$. Therefore, they are all unstable when solving the complex transport Eq. (69).

However, in order to compute $\widetilde{\psi}$ in the absence of a closed-form expression for ψ, the complex transport Eq. (69) has to be solved numerically. Fig. 11 shows that, of all the schemes considered, the Lax-Friedrichs scheme yields the smallest value of $|G|$ for different values of $\Delta Z/\Delta X$. However, the Lax-Friedrichs scheme is not suitable to solve the complex-transport Eq. (69). This can be seen by rewriting the Lax-Friedrichs scheme in the form

$$\frac{P_j^{n+1} - P_j^n}{\Delta Z} + c\frac{P_{j+1}^n - P_{j-1}^n}{2\Delta X} = \frac{\Delta X^2}{2\Delta Z}\frac{P_{j+1}^n - 2P_j^n + P_{j-1}^n}{\Delta X^2}, \tag{77}$$

which represents a finite difference discretization of the equation

$$\widetilde{\psi}_Z + c\widetilde{\psi}_X = \frac{\Delta X^2}{2\Delta Z}\widetilde{\psi}_{XX}. \tag{78}$$

It can be seen that the Lax-Friedrichs scheme introduces numerical diffusion, which is proportional to $\frac{\Delta X^2}{2\Delta Z}$. Since the complex transport Eq. (69) does not contain such a diffusion term, numerical solutions obtained with the Lax-Friedrichs scheme provide an accurate approximation only when $\frac{\Delta X^2}{2\Delta Z}$ is sufficiently small. However, the value of $\Delta Z/\Delta X$ should also be small so that the amplification factor G becomes small, see Fig. 11. Going from Z_n to $Z_{\mathrm{n}+1}$, it has to be remembered that numerical errors are amplified by $|G|$. Therefore, errors in the initial condition at $Z = 0$ are amplified in total by a factor of $|G|^{|Z_{\min}/\Delta Z|} = |G|^N$ when going from $Z = 0$ to $Z = Z_{\min}$. For a given depth $Z_{\min}$, this means that N has to be small to obtain only small numerical errors. However, this requires a relatively large step size ΔZ. Since the ratio $\frac{\Delta Z}{\Delta X}$ should also be small, it must hold $\Delta X > \Delta Z$. This causes the diffusion coefficient $\frac{\Delta X^2}{2\Delta Z}$, which appears in the Lax-Friedrichs scheme given by Eq. (77), to become large. In this case, however, numerical solutions obtained by the Lax-Friedrichs scheme do not accurately approximate the solutions of the complex transport Eq. (69). Therefore, the Lax-Friedrichs scheme is not suitable to approximate solutions of this equation.

Looking again at Fig. 11, it can be seen that the explicit central difference scheme from Eq. (71) yields the second smallest amplification factor among all examined schemes, second only to the Lax-Friedrichs scheme. Consequently, among all presented schemes, the explicit central difference scheme from Eq. (71) should be used to solve Eq. (69) numerically. However, the values of ΔX and ΔZ have to be chosen carefully. If these values are too large, the consistency error $\mathcal{O}(\Delta Z + \Delta X^2)$ will also be large. If the ratio $\Delta Z/\Delta X$ is too large, the amplification factor $|G|$ becomes large, and rounding errors will significantly affect the behavior of the numerical solution. If ΔZ is too small, the number of steps in Z-direction, $N = |Z_{\min}/\Delta Z|$, becomes large, which causes $|G|^N$ to increase significantly. Therefore, it is essential to select ΔX and ΔZ appropriately to ensure reliable results.

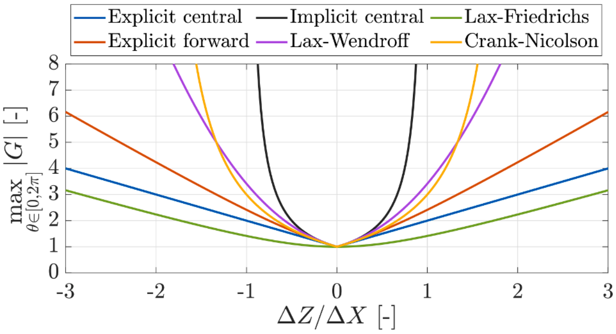

Fig. 11. Amplification factor $|G|$ for different numerical schemes, which are applied to the complex transport Eq. (69). The maximum value of $|G|$ over $\theta \in [0, 2\pi]$ is shown against $\Delta Z/\Delta X$.

5. Conclusion

In this work, the flow field associated with solutions ψ of the nonlinear Schrödinger equation (NLS) is analyzed. Starting with the reconstruction of the corresponding velocity potential ϕ, the behavior of ϕ below the water surface has been investigated. Additionally, different numerical schemes for computing ϕ below the water surface have been analyzed with regard to their stability.

By analyzing several analytical solutions ψ of the NLS, it has been shown that the corresponding velocity potential ϕ can generally become singular at any depth below the water surface. Depending on the solution ψ of the NLS, these singularities may even occur periodically in the vertical direction. Importantly, these singularities are not physical blow-ups of the fluid flow but purely mathematical artifacts. They arise from the analytic continuation of the wave envelope ψ from the real spatial coordinate into the complex spatial plane and indicate the limited domain of validity of the analytic continuation.

Physically, the NLS is effective for modeling nonlinear deep-water waves with a narrow spectral bandwidth and moderate wave steepness. However, the associated flow field below the water surface can contain unrealistic singularities. These singularities have no physical meaning but instead reflect the limitations of the modeling approach. Therefore, care is needed when interpreting flow fields associated with solutions ψ of the NLS.

Furthermore, it has been shown that the numerical computation of the auxiliary variable $\widetilde{\psi}$, which appears in the calculation of the velocity potential ϕ, can become a big issue due to numerical instability. Various schemes have been investigated to compute $\widetilde{\psi}$ numerically, and all of them lack numerical stability. As a result, small incoming errors like rounding errors can amplify and dominate the behavior of the numerical solution at greater depths.

From an engineering perspective, these findings emphasize the importance of developing more stable and robust algorithms, along with careful error management, for the numerical computation of flow fields associated with solutions ψ of the NLS. This is especially important for engineering applications involving deeper structures. Furthermore, it is advisable to restrict computations of the velocity potential ϕ to depths above any singularities. Recognizing these limitations is essential for ensuring reliable simulations and robust engineering decisions in offshore design processes.

In summary, while the NLS is effective for surface wave modeling under the assumptions of narrow spectral bandwidth and moderate wave steepness, its associated flow field below the water surface involves mathematical singularities and numerical challenges. These findings should be carefully considered both in the physical interpretation and in engineering applications when dealing with the flow field of water waves corresponding to the NLS.

CRediT authorship contribution statement

Marten Hollm: Writing – original draft, Visualization, Validation, Software, Investigation, Formal analysis, Conceptualization; **Robert Seifried:** Writing – review & editing, Supervision, Funding acquisition, Formal analysis, Conceptualization.

Declaration of competing interest

The authors declare that they have no known competing financial interests or personal relationships that could have appeared to influence the work reported in this paper.

Acknowledgements

The authors would like to thank the German Research Foundation (DFG) for the financial support of the project 528383251.

References

Akhmediev, N., Ankiewicz, A., 1993. Spatial soliton X-junctions and couplers. Opt. Commun. 100 (1-4), 186–192. https://doi.org/10.1016/0030-4018(93)90577-R

Akhmediev, N., Ankiewicz, A., 1997. Solitons: Non-Linear Pulses and Beams. Chapman and Hall.

Akhmediev, N., Ankiewicz, A., Soto-Crespo, J.M., 2009. Rogue waves and rational solutions of the nonlinear Schrödinger equation. Phys. Rev. E-Stat. Nonlinear Soft Matter Phys. 80 (2), 026601. https://doi.org/10.1103/PhysRevE.80.026601

Akhmediev, N., Eleonskii, V.M., Kulagin, N.E., 1985. Generation of periodic trains of picosecond pulses in an optical fiber: exact solutions. Sov. Phys. JETP 62 (5), 894–899.

Akhmediev, N.N., Korneev, V.I., 1986. Modulation instability and periodic solutions of the nonlinear Schrödinger equation. Theor. Math. Phys. 69 (2), 1089–1093. https://doi.org/10.1007/BF01037866

Bludov, Y.V., Konotop, V.V., Akhmediev, N., 2009. Matter rogue waves. Phys. Rev. A 80 (3), 033610. https://doi.org/10.1103/PhysRevA.80.033610

Carter, J.D., Curtis, C.W., Kalisch, H., 2020. Particle trajectories in nonlinear Schrödinger models. Water Waves 2, 31–57. https://doi.org/10.1007/s42286-019-00008-7

Chabchoub, A., 2013. An Experimental Study on Breathers in Water Waves. Ph.D. thesis, Hamburg University of Technology.

Chabchoub, A., Akhmediev, N., Hoffmann, N.P., 2012. Experimental study of spatiotemporally localized surface gravity water waves. Phys. Rev. E 86 (1), 016311. https://doi.org/10.1103/PhysRevE.86.016311

Dostal, L., Hollm, M., Kreuzer, E., 2020. Study on the behavior of weakly nonlinear water waves in the presence of random wind forcing. Nonlinear Dyn. 99 (3), 2319–2338. https://doi.org/10.1007/s11071-019-05416-5

Dudley, J.M., Dias, F., Erkintalo, M., Genty, G., 2014. Instabilities, breathers and rogue waves in optics. Nat. Photonics 8, 755–764. https://doi.org/10.1038/NPHOTON.2014.220

Dysthe, K.B., 1979. Note on a modification to the nonlinear Schrödinger equation for application to deep water waves. Proc. R. Soc. A 369, 105–114. https://doi.org/10.1098/rspa.1979.0154

Dysthe, K.B., Trulsen, K., 1999. Note on breather type solutions of the NLS as models for freak-waves. Phys. Scr. T82, 48–52. https://doi.org/10.1238/Physica.Topical.082a00048

El-Tantawy, S.A., Salas, A.H., Alyousef, H.A., Alharthi, M.R., 2022. Novel approximations to a nonplanar nonlinear Schrödinger equation and modeling nonplanar rogue waves/breathers in a complex plasma. Chaos Solitons Fractals 163, 112612. https://doi.org/10.1016/j.chaos.2022.112612

Gaillard, P., 2013. Degenerate determinant representation of solutions of the nonlinear Schrödinger equation, higher order Peregrine breathers and multi-rogue waves. J. Math. Phys. 54 (1). https://doi.org/10.1063/1.4773096

Greaves, D., Iglesias, G., 2018. Wave and Tidal Energy. Hoboken, NY: John Wiley & Sons. https://doi.org/10.1002/9781119014492

Hollm, M., 2025. A New Computational Method for the Fluid-Structure Interaction in Random Nonlinear Ocean Waves. Ph.D. thesis, Hamburg University of Technology. https://doi.org/10.15480/882.14990

Hollm, M., Dostal, L., Carter, J.D., Seifried, R., 2024. Determination of particle paths and hydrodynamic forces of random wind forced nonlinear ocean waves. Proc. Inst. Mech. Eng., Part M 238 (2), 406–416. https://doi.org/10.1177/14750902231196812

Hollm, M., Dostal, L., Fischer, H., Seifried, R., 2021. Study on the interaction of nonlinear water waves considering random seas. Proc. Appl. Math. Mech. 20 (1), e202000307. https://doi.org/10.1002/pamm.202000307

Hollm, M., Dostal, L., Seifried, R., 2022. Hydrodynamic forces acting on cylindrical piles subjected to wind-forced random nonlinear water waves. In: Lacarbonara, W., Balachandran, B., Leamy, M.J., Ma, J., Tenreiro Machado, J.A., Stepan, G. (Eds.), Advances in Nonlinear Dynamics. Springer International Publishing, Cham, pp. 95–105.

Hollm, M., Seifried, R., 2026. A computational method for the fluid-structure interaction in nonlinear ocean waves using the nonlinear Schrödinger equation. Ocean Eng. 343, 123418. https://doi.org/10.1016/j.oceaneng.2025.123418

Kuznetsov, E.A., 1977. Solitons in a parametrically unstable plasma. Sov. Phys. Dokl. 22, 507–508.

Langtangen, H.P., 2003. Computational Partial Differential Equations: Numerical Methods and Diffpack Programming. Berlin, Heidelberg: Springer. 2 edition. https://doi.org/10.1007/978-3-642-55769-9

LeVeque, R.J., 1992. Numerical Methods for Conservation Laws. Basel: Birkhäuser. 2 edition. https://doi.org/10.1007/978-3-0348-8629-1

Lin, P., 2008. Numerical Modeling of Water Waves. London, New York: Taylor & Francis. https://doi.org/10.1201/9781482265910

Ma, Y.-C., 1979. The perturbed plane-wave solutions of the cubic Schrödinger equation. Stud. Appl. Math. 60 (1), 43–58. https://doi.org/10.1002/sapm197960143

Marsal, D., 1976. Die Numerische Lösung Partieller Differentialgleichungen in Wissenschaft und Technik. Mannheim, Wien, Zürich: Bibliographisches Institut.

Mei, C.C., 1983. The Applied Dynamics of Ocean Surface Waves. New York: John Wiley & Sons.

Newman, J.N., 2018. Marine Hydrodynamics. Cambridge: The MIT press.

Onorato, M., Osborne, A.R., Serio, M., Bertone, S., 2001. Freak waves in random oceanic sea states. Phys. Rev. Lett. 86 (25), 5831–5834. https://doi.org/10.1103/PhysRevLett.86.5831

Osborne, A.R., 2010. Nonlinear Ocean Waves and the Inverse Scattering Transform. Amsterdam: Academic Press. 1 edition.

Peregrine, D.H., 1983. Water waves, nonlinear Schrödinger equations and their solutions. J. Aust. Math. Soc. Ser. B Appl. Math. 25 (1), 16–43. https://doi.org/10.1017/S0334270000003891

Satsuma, J., Yajima, N., 1974. B. Initial value problems of one-dimensional self-modulation of nonlinear waves in dispersive media. Prog. Theor. Phys. Suppl. 55, 284–306. https://doi.org/10.1143/PTPS.55.284

Shao, Y., Zheng, Z., Liang, H., Chen, J., 2022. A consistent second-order hydrodynamic model in the time domain for floating structures with large horizontal motions. Comput.-Aided Civ. Infrastruct. Eng. 37 (7), 894–914. https://doi.org/10.1111/mice.12782

Shrira, V.I., Geogjaev, V.V., 2010. What makes the Peregrine soliton so special as a prototype of freak waves? J. Eng. Math. 67, 11–22. https://doi.org/10.1007/s10665-009-9347-2

Slunyaev, A., Clauss, G.F., Klein, M., Onorato, M., 2013. Simulations and experiments of short intense envelope solitons of surface water waves. Phys. Fluids 25 (6), 067105. https://doi.org/10.1063/1.4811493

Tveito, A., Winther, R., 1998. Introduction to Partial Differential Equations: A Computational Approach. New York: Springer. https://doi.org/10.1007/b98967

Witt, A., 2019. Inducing Predefined Nonlinear Rogue Waves on Basis of Breather Solutions. Ph.D. thesis, Hamburg University of Technology. https://doi.org/10.15480/882.2224

Zakharov, V.E., 1968. Stability of periodic waves of finite amplitude on the surface of a deep fluid. J. Appl. Mech. Tech. Phys. 9 (2), 190–194. https://doi.org/10.1007/BF00913182

Zakharov, V.E., Gelash, A.A., 2013. Nonlinear stage of modulation instability. Phys. Rev. Lett. 111 (5), 054101. https://doi.org/10.1103/PhysRevLett.111.054101